Univerzita Karlova v Praze
Matematicko-fyzikální fakulta

DIPLOMOVÁ PRÁCE

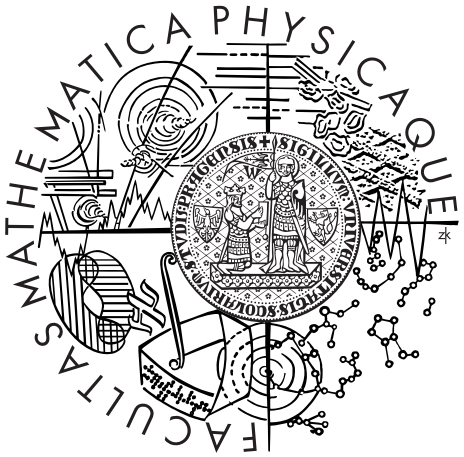

Martin Čochner

Elektromagnetická indukce: 3-D modelování nespojitou Galerkinovou metodou

Katedra geofyziky

Vedoucí diplomové práce: RNDr. Jakub Velímský Ph.D.

Studijní program: fyzika

Studijní obor: matematické a počítačové modelování ve fyzice a technice

Praha 2012

Rád by som predovšetkým poďakoval vedúcemu mojej diplomovej práce Mgr. Jakobuvi Velímskému, PhD za trpezlivosť, nepostradateľné rady, motiváciu, podporu a za všetok čas, ktorý mi venoval počas dlhého obdobia vzniku tejto práce. Tiež by som rád poďakoval Mišovi a Helen za korekcie. Hlavne by som rád poďakoval mojej rodine za neustálu podporu, ktorej sa mi dostávalo počas celého môjho štúdia.

I would also like to thank to Jastin, who explained me the source of spurious solutions in Maxwell's equations. Next, I would like to thank to developers of *deal.ii* library and, among them, especially to Wolfgang Bangerth for providing quick and clear support on the mail list. My thanks also goes to all creators of free software that was used in this thesis; Linux, Inkspace, Paraview, LaTeX, and others.

And, last but definitely not least, I would like to thank to Maira for all the support.

Prehlasujem, že som svoju diplomovú prácu vypracoval samostatne a výhradne s použitím citovaných prameňov, literatúry a ďalších odborných zdrojov.

Beriem na vedomie, že sa na moju prácu vzťahujú práva a povinnosti vyplývajúce zo zákona č. 121/2000 Sb., autorského zákona v platnom znení, obzvlášť skutočnosť, že Univerzita Karlova v Praze má právo na uzavretie licenčnej zmluvy o užití tejto práce ako školského diela podľa §60 odst. 1 autorského zákona.

V ..... dňa .....

Název práce: Elektromagnetická indukce: 3-D modelování nespojitou Galerkinovou metodou

Autor: Martin Čochner

Katedra: Katedra geofyziky

Vedoucí diplomové práce: RNDr. Jakub Velímský Ph.D., katedra geofyziky

Abstrakt: Táto práca sa zaoberá numerickým modelovaním elektromagnetickej indukcie v 3D prostredí s heterogénnym rozložením vodivosti. Maxwellove rovnice v kvazistacionárnom priblížení riešime pomocou spojitých a nespojitých konečných elementov. Diskutujeme ich implementáciu v numerickej knižnici *deal.ii*. Numerické výsledky porovnávame navzájom a tiež s kvázianalytickým riešením, pre 1D heterogénneho rozloženia vodivosti. Diskutujeme použité numerické metódy, limity nášho kódu pre praktické použitie a možné vylepšenia kódu.

Klíčová slova: 3-D modelovanie, CSEM, elektromagnetická indukcia

Title: Electromagnetic induction: 3-D modelling using the discontinuous Galerkin method

Author: Martin Čochner

Department: Department of Geophysics

Supervisor: RNDr. Jakub Velímský Ph.D., Department of Geophysics

Abstract: This work deals with numerical modeling of electromagnetic induction in 3D environment with heterogeneous conductivity. We develop a program to solve Maxwell's equations in quasistatic approximation by using Continuous and Discontinuous Finite Elements. Their implementation in the numerical library *deal.ii* is discussed. The obtained numerical results are compared with each other and also with a quasianalytic solution for an environment with 1D heterogeneous conductivity. We discuss different numerical methods, limits of our code for practical use and possible future enhancements.

Keywords: three-dimensional modelling, CSEM, electromagnetic induction

Contents

Preface

Seismic, *potential field*, and *electromagnetic* (EM) methods are the three principal tools of applied geophysics. *Controlled Source Electromagnetic* (CSEM) methods belong to the class of EM methods which use artificially produced EM fields[1]. CSEM has a wide spectrum of applications that include mineral exploration, hydrogeological applications, mapping and detection of land mines, hydrocarbon prospecting, as well as others.

In this work, we focused our attention on one interesting example of hydrocarbon prospecting in the offshore environment. It is one of the more recent application of CSEM and it is commonly known as marine Controlled Source Electromagnetics (mCSEM). Electromagnetic waves are sent by a transmitter that is towed by a vessel and typically located a few meters (10-100 m) above the sea-floor. This transmitter operates at frequencies in the range of 0.25Hz-1.25Hz in order for electromagnetic waves to reach long distances. Measurements are recorded by a set of receivers located along the sea-floor at distances up to 20 km from the source. Our objective is to accurately simulate marine CSEM measurements at the receivers. These measurements can be later used for inversion in order to characterize the reservoir.

The goal of this thesis is to develop a program for *forward modeling* CSEM in a heterogeneous 3-D conductivity environment. The forward problem can be stated in a time domain or reformulated (and simplified), by using the Fourier transformation, in the frequency domain. In the frequency domain, there are many, even freely available, FEM codes solving the CSEM forward problem. Using the time domain measurements has the advantage of shortening the time of the field campaign. In recent years, the time domain field measurements in the marine environment are gaining popularity as described by Constable and Srnka (2007) and more recently by Constable (2010). Therefore, we aim the focus of this work on the development of CSEM forward solver in the time domain. We also investigated the use of *Discontinuous Galerkin* (DG) method, which is a variant of *finite element method* where the test and trial functions are discontinuous and the coupling between elements are enforced only weakly.

This thesis consists of 4 chapters. The beginning of *Chapter 1* introduces the physics of CSEM, reviews the Maxwell equations and also their weak formulation. The weak formulation then creates the basis for subsequent discretization of equations. *Chapter 2* introduces one type of nonconforming spatial discretization, the Discontinuous Galerkin method, and also a more traditional conforming discretization using so-called *Nédélec elements*. A substantial part of the thesis is developing a program that would practically test these numerical formulation. This program together with the most important decisions regarding its implementation is discussed in *Chapter 3*. Lastly, we carry out the numerical tests of developed program against known solutions and discuss the result in *Chapter 4*.

[1] in contrast to the magnetoteluric (MT) method that uses naturally occurring EM fields

1. Introduction

1.1 CSEM as a method of geophysical research

Linear electromagnetic properties of matter are, in simple material models usually used in applied geophysics, described by three material quantities: *electric permitivity* ε, *magnetic permeability* μ, and electric *conductivity* σ. Electric permitivity ε is not considered in our *quasistatic approximation* that sufficiently describes all electromagnetic phenomena at the lower frequencies. Most of the materials in the ground are nonmagnetic and therefore the permeability of most of the materials is close to the *permeability of free space* μ_0 (e.g. Telford, 1990). On the other hand, the conductivity is a physical parameter with one of the highest dynamic range in the nature. For materials in the Earth, it varies from 10^{-18} S/m (diamond) to 10^7 S/m (copper), i.e., by 25 orders of magnitude (Tezkan, 1999). All the EM methods used in geophysics observe the conductivity distribution in the subsurface.

The basic physics of CSEM can be described as the electric current of the source, which causes, through electromagnetic coupling or directly, the flow of electric currents in the ground. This electric and magnetic response of the ground is measured by receivers.

There are many criteria to distinguish different types of CSEM. As these methods implicate different mathematical descriptions it is useful to introduce them.[1]

There are two ways how energy from the source can enter the ground: induction-magnetic and galvanic-electric. In the case of an *electric* source, the current from a battery or electric generator directly flows to the ground through electrodes galvanically connected to the ground.[2] In the case of a *magnetic* source, the current from the generator flows only in the attached coil and does not directly enter the ground. The magnetic field from a coil induces, through Faraday's law, an electric current in the conductive media. We are generally interested in the cases when the current from the source is not steady.

Whether the current from the source is time-harmonic or has more general time dependency it can be preferable to solve the forward problem in the *frequency-domain*, or to leave the time dependence in ME and solve ME in *time-domain*. In general, it is common to use Fourier transformation also for more complicated sources with a wide frequency spectrum and to solve many time-harmonic forward problems.

CSEM has a wide spectrum of applications including mineral exploration, hydrocarbon prospecting, hydrogeological applications, hazardous waste mapping and detection of land mines (Everett, 2012). After years of belief that CSEM is not suited for an offshore environment, because the high electrical conductivity of sea water preclude the application of electromagnetic systems for exploration, the marine CSEM is becoming more popular and is extensively and successfully used for hydrocarbon and hydrates prospecting (e.g. Edwards (2005) and Constable

[1] also the specific geophysical terms

[2] If the current between the electrodes is steady we can directly measure bulk resistivity between electrodes of the generator. In geophysical literature it is called *direct current* method.

and Srnka (2007)).

We have to note that although we simulate the EM fields in an inhomogenous 3-D field, this is usually not the final goal in the praxis. The ultimate goal of most of the CSEM computations is the so-called *inverse problem*. There, using our model for concrete description, given a time series of measured EM from the receivers (Figure 1.1), we need to recover the conductivity under the seafloor. In other words, we are trying to find such conductivity model, that minimizes the differences between data observed at the receivers, and signals predicted for that model by the forward solution. It leads to the ill-posed problem that is solved by regularization. This problem is harder than the forward problem that is discussed in this work. However, having a stable and fast forward problem solver is necessary during a inverse process. The review of possible approaches to the inverse problem in CSEM can be find in the review papers by Avdeev (2005) and Everett (2012).

We take a marine CSEM with horizontally deployed electric dipole as a model problem for this work.

1.2 Physical model

An electromagnetic transmitter is towed close to the seafloor to maximize the coupling of electric and magnetic fields with seafloor. These fields are recorded by instruments deployed on the seafloor at some distance from the transmitter Constable and Srnka (2007). This scenario is shown in Figure 1.1.

The basic types of sources are electric or magnetic dipoles, which are usually oriented either horizontally or vertically in the sea. Hydrocarbon reservoirs often form resistive bodies whose thickness is much less than its depth of burial below the measurement surface. To create a measurable response from such an object it is necessary to generate currents that are normal to the boundaries (Um and Alumbaugh, 2007). A vertical magnetic dipole, for example, would excite mainly horizontal current flows. For the same reason, the magnetotelluric method cannot be used for their detection. Horizontal magnetic dipoles also excite both vertical and horizontal currents, but are less favored than electric dipoles for operational reasons. The solution for this problem is to turn our attention to electrical dipole sources, in particular horizontal electric dipole (HED) (Constable and Srnka 2007; Um and Alumbaugh 2007).

In the previous paragraph we justified our focus to use of horizontally deployed electric dipole as our source of electric current. Now we introduce a concept that is physically important in CSEM and also later gives us a hint about the size of the computation domain Ω.

It is known (Zhdanov, 2009) that the electric field from the source is exponentially attenuated as it enters($z \to +\infty$) the conductive material obeying the equation

$$E(z) = E_0 \exp[-\frac{z}{\delta} - i\frac{z}{\delta}], \tag{1.1}$$

$$\delta(f, \sigma) = \frac{1}{\sqrt{\mu_0 \sigma \pi f}} \tag{1.2}$$

where the electrical field $\boldsymbol{E}$ with the frequency f [Hz] propagates deeper into the

material with the conductivity σ [S/m] as $z \to +\infty$. Frequency f together with the conductivity σ in defines δ in (1.2) as the *standard depth of penetration*, (Zhdanov 2009; Simpson and Bahr 2005). For an electric source with the frequency f and conductivity σ penetration depth gives us the thickness of the material that attenuates the magnitude of the initial field to $1/e \sim 0.367$.

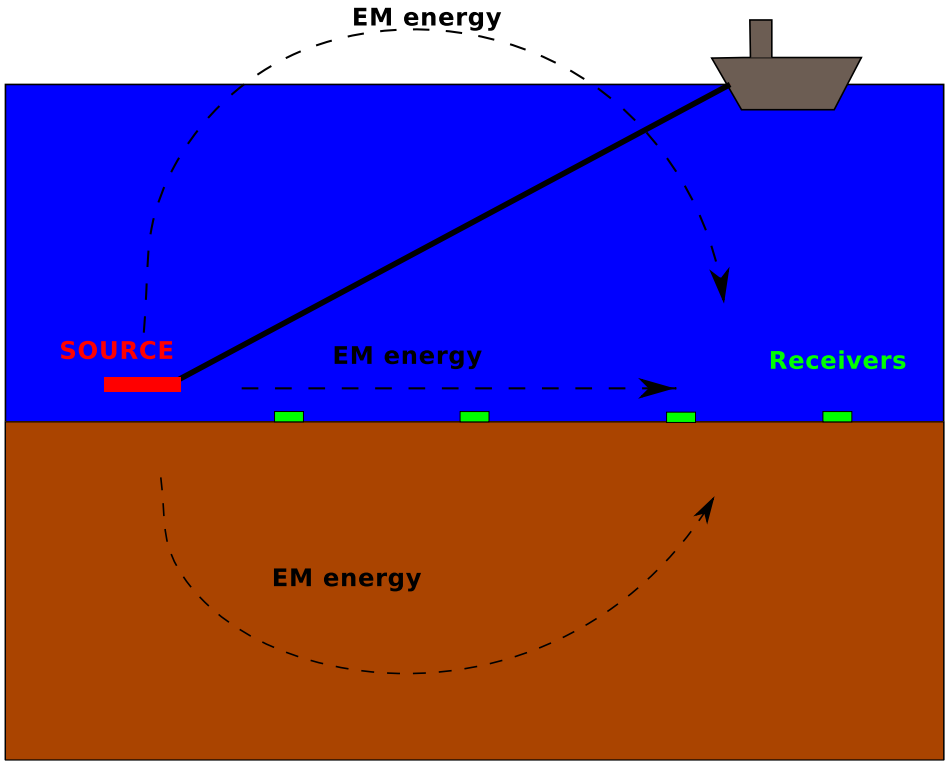

Figure 1.1: Physical model of a marine control source electromagnetic induction.

1.3 Literature overview

In this section we will give a short overview of the previous approaches. We mostly follow the review articles by (Avdeev, 2005) and (Everett, 2012), and references therein.

Modeling of CSEM belongs naturally into the *computational electromagnetic*, which is a vast field with many important applications in everyday life. The amount of problems that can be solved by analytical methods is very limited which had lead to development of many numerical techniques. Some specific problems can be very effectively solved by particular solvers (e.g. thin sheets approximation or integral equation approach) but for a general 3-D conductivity problems the most commonly used methods are the Finite Difference and Finite element methods (Avdeev, 2005).

The Finite Difference (FDM) and Finite Element (FEM) methods are the most common choices when simulating EM fields with general 3-D material description. The advantage of Finite-Difference is its relatively simple implementation, with the most prominent representant the Yee algorithm. The algorithm proposed by Yee (1966) discretises first order Maxwell's equations based on the regular Cartesian mesh. Staggered grid (Fig. 1.2) combined with the Du Fort-Frankel

leap-frog time marching process, leads to the fully explicit numerical scheme. The avoidance of matrix computations and simplicity can be exploited in a very efficient parallel implementation. The leap-frog time marching process is only conditionally stable and must obey the well known *Courant-Fridrichs-Levy* (CFL) condition. When the domain can be effectively covered by a regular Cartesian grid, the Yee's algorithm is heavily used, also among the engineering community (Jin, 2002).

On the other hand the Maxwell equations in conductive matter have parabolic behavior. The CFL condition is too restrictive in the time-marching process and thereby renders direct application of Yee's algorithm impossible. The problem was partially solved by Wang and Hohmann (1993). The use of an artificially high electrical permittivity allows reduction of the computer time. The parallel implementation of the same algorithm is discussed in (Commer and Newman, 2004).

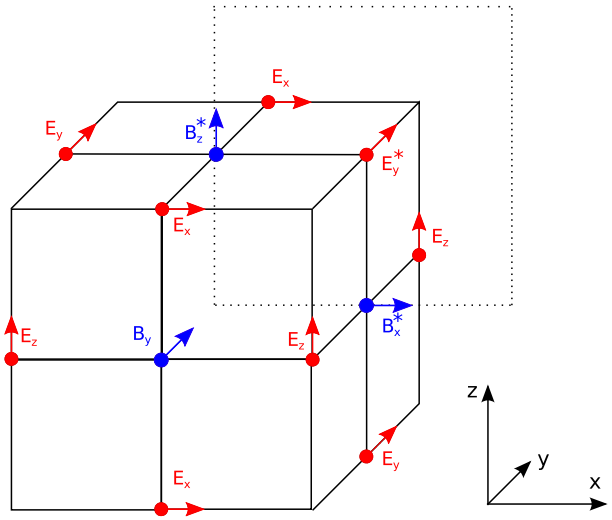

Figure 1.2: Example of one cell of a staggered grid by Yee (1966). Components of the vector $\boldsymbol{E}$ on this cell are evaluated only on the edges. On the other side the components of the vector $\boldsymbol{B}$ are evaluated on the faces of the cell. This scenario gives a framework to intuitively evaluate line integrals of $\boldsymbol{E}$ and corresponding face integrals of $\boldsymbol{B}$ and the integral form of Faraday's Law $\int_\Omega \nabla \times E = \int_\Omega \partial_t B$ can be discretized. The dashed line depicts one face of a "staggered" cell with starred vector components on this face. The roles of the vector components are interchanged. In the "staggered" face the $\boldsymbol{E}$ resides on the faces and $\boldsymbol{B}$ resides on the edges. The discretization of Ampere's Law comes similar as in the case of Faraday's Law.

The second numerical method that is commonly used for CSEM forward computations is the finite element method (FEM). In FEM, the EM field (either directly electric and magnetic fields or through its potentials) is decomposed to some basic functions on smaller domains called elements. Generally, the main advantage of finite element methods is considered to be the geometrical flexibility, because the complex geological structures can be covered by an unstructured mesh. This is an advantage to the stair-step approximation employed in FDM (Jin, 2002). Also, when FDM methods are based on the strong formulation of partial differential equations, FEM methods are developed within the framework

of the weak formulation. This allows to prove the existence of the discrete solution, and also to develop rigorous a posteriori error estimates which are valuable in adaptive methods. Both are either difficult or impossible to do in FDM.

Various formulations have been developed using different forms of EM equations. Coupled first order Maxwell's equations, scalar and vector potentials with (or without) a gauge condition and the second order electric or magnetic equations.

Methods based on the coupled first order Maxwell's equations compute directly both electric and magnetic components of EM field. That can be very convenient if both fields are needed. The disadvantage is a larger memory cost. Vector potential formulation allows the use of traditional Lagrange elements (Badea et al., 2001), (Velímský and Martinec, 2005). Moreover, by implicitly implying divergence constraints the primary fields are free of the so called *spurious* solutions, which is otherwise a serious problem in electromagnetic modeling. On the other side it can be problematic to recover physically relevant primary fields. The second order wave equation has the advantage that it only solves for the electric or magnetic fields thus minimizing the total number of parameters to solve (Um et al., 2010). The high order FEM approximation are more complicated from implementation point of view, but the need for solving many large problems is eminent and lately the *hp goal-oriented* FEM methods in the frequency domain have been successfully used in CSEM forward modeling (Pardo et al. 2006; Pardo et al. 2007).

Most of the published papers for geophysical time domain[3] simulations (Everett and Edwards 1993, Börner et al. 2008) solve the ME in the frequency domain for many frequencies. Afterwards, the obtained results are transfered back to the time domain. Direct time domain computations are less popular because they lead to the system of linear algebra equations that needs to be inverted at every time step thus carrying a hight computational cost. Nevertheless, Um et al. (2010) successfully implemented such an approach. He partially diminished the overall computational cost by employing a direct solver. To some extent we follow its approach, but we are using different shape elements and a preconditioned iterative solver.

The overview and discussion of implemented Discontinuous Galerkin method is postponed to Chapter 2.

1.4 Maxwell's equations

1.4.1 Maxwell's equations - the classical form

Models of electromagnetic induction belong under the phenomena of classical electrodynamics and are described by the Maxwell equations. These equations are traditionally written in the form of four partial differential equations (e.g.

[3] also *transient*

Monk, 2003) and read as

$$\nabla \times \boldsymbol{E} = -\frac{\partial \boldsymbol{B}}{\partial t}, \tag{1.3}$$

$$\nabla \times \boldsymbol{H} = \boldsymbol{j} + \frac{\partial \boldsymbol{D}}{\partial t}, \tag{1.4}$$

$$\nabla \cdot \boldsymbol{D} = \rho, \tag{1.5}$$

$$\nabla \cdot \boldsymbol{B} = 0, \tag{1.6}$$

where vector fields $\boldsymbol{E}$, $\boldsymbol{H}$, $\boldsymbol{B}$, $\boldsymbol{D}$, $\boldsymbol{j}$ and scalar field ρ are functions of position $\boldsymbol{x} \in \mathbb{R}^3$ and time t. We recall that $\boldsymbol{E}$ denotes the electric field, $\boldsymbol{H}$ is the magnetic field strength, $\boldsymbol{B}$ is the magnetic flux density also called magnetic induction, $\boldsymbol{D}$ represents electric displacement, $\boldsymbol{j}$ is the density of electric current, and ρ is the free-charge density.

Taking divergence of Faraday's law (1.3)

$$\nabla \cdot (\nabla \times \boldsymbol{E}) = -\nabla \cdot \frac{\partial \boldsymbol{B}}{\partial t}$$

yields

$$\frac{\partial \nabla \cdot \boldsymbol{B}}{\partial t} = 0. \tag{1.7}$$

We see that if $\nabla \cdot \boldsymbol{B} = 0$ for t = 0 then $\nabla \cdot \boldsymbol{B} = 0$, $t \in [0, \mathrm{T}]$. It is important for any discretization to confine with this constraint.

Taking divergence of Ampere's law (1.4)

$$\nabla \cdot (\nabla \times \boldsymbol{H}) = \nabla \cdot \boldsymbol{j} + \nabla \cdot \frac{\partial \boldsymbol{D}}{\partial t}$$

yields the conservation equation for charge

$$\frac{\partial \rho}{\partial t} + \nabla \cdot \boldsymbol{j} = 0 \tag{1.8}$$

We see that four ME are not independent, but the divergence equations (1.5-1.6) can be understood as necessary conditions for the other tuple of equations (1.3 - 1.4) that stand for Faraday's and Ampére-Maxwell's law. If the initial conditions satisfy the divergence constraints then the solution of Maxwell's equations will also satisfy the divergence constraints.

The definitions of differential operators grad, div, and curl from previous equations (1.3 - 1.5) are classically defined only on smooth $(\mathrm{C}^1(\Omega))^3$ functions. Between the materials with non continuous material properties as well as at the boundaries of the computational domain, the boundary conditions must be provided (Monk, 2003).

Interface and boundary conditions

When the Maxwell equations are understood in the classical (strong) sense the equations holds only inside the domain with continuously varying material constants. In general, the electromagnetic fields $\boldsymbol{E}$, $\boldsymbol{B}$, $\boldsymbol{D}$, and $\boldsymbol{H}$ can be discontinuous at a boundary between two different media, or at a surface that carries

charge density ρ_s or current density $\boldsymbol{j}_s$. First we introduce the jump of a (vector) function $u(\boldsymbol{r})$ across the interface Σ as

$$[u(\boldsymbol{r})]^+_- = u^+(\boldsymbol{r}) - u^-(\boldsymbol{r}), \text{ where} \tag{1.9}$$
$$v^- = \lim_{\delta \to 0+} v(\boldsymbol{r} - \delta \boldsymbol{n}) \text{ and} \tag{1.10}$$
$$v^+ = \lim_{\delta \to 0+} v(\boldsymbol{r} + \delta \boldsymbol{n}). \tag{1.11}$$

The boundary conditions across surface discontinuities can be derived from the integral form of Maxwell's equations (e.g. Griffiths, 1999) and read as

$$[\boldsymbol{n} \times \boldsymbol{E}]^+_- = 0, \tag{1.12}$$
$$[\boldsymbol{n} \cdot \boldsymbol{B}]^+_- = 0, \tag{1.13}$$
$$[\boldsymbol{n} \times \boldsymbol{H}]^+_- = \boldsymbol{j_s}, \tag{1.14}$$
$$[\boldsymbol{n} \cdot \boldsymbol{D}]^+_- = \rho_s, \tag{1.15}$$

where $\boldsymbol{n}$ is outer unit normal vector of the interface Σ, $\boldsymbol{j_s}$ is density of free *surface* currents and $\boldsymbol{\rho_s}$ is density of free (imposed) surface charges.

We note, that whenever in the following text, we see the boundary value problem or initial boundary value problem we expect that this problem has to be understood *together with* all interface conditions (1.12 - 1.15). Fortunately, when we work with the weak formulation, all these interface conditions implicitly hold (Bossavit, 1998).

Constitutive relations

Under the assumption of linear material, the four vector fields $\boldsymbol{E}$, $\boldsymbol{H}$, $\boldsymbol{B}$, $\boldsymbol{D}$ are further tied up with constitutive equations:

$$\boldsymbol{D} = \varepsilon \boldsymbol{E} \tag{1.16}$$
$$\boldsymbol{B} = \mu \boldsymbol{H} \tag{1.17}$$

where ε and μ are permittivity and magnetic permeability. Generally ε and μ are positive definite tensors. When the material is isotropic the tensors degenerate to scalars.

The last constitutive relation needs to be posted for conducting materials, where the electromagnetic field itself gives rise to currents. In most geophysical simulation it's customary to use a linear relation; *Ohm's law*. As our model also consists of generators we introduce the generalized version of Ohm's law (Bossavit, 1998) and we have for total current density

$$\boldsymbol{j} = \sigma \boldsymbol{E} + \boldsymbol{j^g}, \tag{1.18}$$

where σ is called *conductivity* and $\boldsymbol{j^g}$ denotes *given* (or *impressed*) current of the source. Conductivity is nonnegative scalar[4] function of place vanishing on insulators. Given current is a vector function of place and time describing applied current and is vanishing outside the generator.

[4] in the case of anisotropic materials σ can be a 2nd rank symmetric tensor (Zhdanov, 2009)

Dumped wave equation

When we differentiate Ampére-Maxwell's law (1.4) with respect to the time and use our linear constitutive relations (1.16 - 1.18) we can eliminate the magnetic term $\mu^{-1}\frac{\partial B}{\partial t}$ by using Faraday's law (1.3). Afterwards, we have a dumped wave equation in $\boldsymbol{E}$ which reads as

$$\varepsilon\frac{\partial^2 \boldsymbol{E}}{\partial t^2} + \sigma\frac{\partial \boldsymbol{E}}{\partial t} + \nabla \times (\mu^{-1}\nabla \times \boldsymbol{E}) = -\frac{\partial \boldsymbol{j^g}}{\partial t} \qquad \boldsymbol{x} \in \Omega \subset \mathbb{R}^3 \tag{1.19}$$

If we choose to eliminate electrical field instead we would get similar vector wave equation where the primary vector field is $\boldsymbol{H}$ (Zhdanov, 2009). The main difference between the formulations is the source term and the boundary conditions (Rieben and White, 2006). In our case of electrical dipole source it is advantageous to use formulation where the electric field is the primary unknown.

1.5 Magnetoquasistatic model

The entirety of electrodynamics is described by the hyperbolic system of the Maxwell equations (1.3)-(1.5), which models a wide spectrum of natural phenomena e.g. electrostatic fields, magnetostatic fields, electricity in power lines, EM waves and others. Solving full Maxwell's equations (especially in three dimensions) can be numerically expensive and, often, not necessary as simplified models can provide the same[5] or acceptable accuracy. These models can be *static* (EM field are static), *quasistatic* and also *high-frequency approximation* (considering air as vacuum). CSEM, together with the most methods used in geophysics, fits very well into the quasistatic approximation Zhdanov (2009). A thorough discussion regarding different quasistatic approximations can be found in Larsson (2007). We use the most common magneto-quasistatic model described by neglecting the Maxwell displacement current in the Maxwell-Ampere law (1.4). By incorporating the material relations our model is described by (1.4, 1.5 a 1.6) and the Ampere law

$$\nabla \times \boldsymbol{H} = \boldsymbol{j^g} + \sigma\boldsymbol{E}. \tag{1.20}$$

Applying divergence to Ampere law (1.20)

$$\nabla \cdot (\boldsymbol{j^g} + \sigma\boldsymbol{E}) = 0 \tag{1.21}$$

and comparing to equation of charge conservation (1.8), which was the the direct result of full Maxwell's equations, we see that the charge is not conservative and the quasistatic approximation holds only if

$$\frac{\partial \rho}{\partial t} \approx 0. \tag{1.22}$$

It is known that most of the materials found in the nature are nonmagnetic. In this case we can write in (1.17) $\mu = \mu_0$,

$$\boldsymbol{B} = \mu_0\boldsymbol{H} \tag{1.23}$$

[5] within the computational error

For the sake of simplicity, we will equip our model with homogeneous Dirichlet boundary conditions. This condition physically corresponds to the idealization when the boundary of Ω is created by a perfect electric conductor. Such a claim is a crude, but commonly used, simplification in geophysical literature (Commer and Newman 2004; Um et al. 2010). It can be justified by the fact that the boundary conditions are negligible when choosing "big enough" domain. A good hint about the size of domain can give the penetration depth introduced in (1.2), which is dependent on the frequency of the source and also the conductivity in the model. Therefore, the size of domain will be dependent on the frequency of the source, as well as on the conductivity of the domain.

To sum up, we have the following strong formulation for the initial-boundary value problem for the Maxwell equations in the magneto-quasistatic approximation:

(*Strong formulation, primary field*):
Find vector electric intensity $\boldsymbol{E}(x,t)$ in (0, T) such that it holds:

$$\sigma\frac{\partial \boldsymbol{E}}{\partial t} + \nabla \times (\mu^{-1}\nabla \times \boldsymbol{E}) = -\frac{\partial \boldsymbol{j^g}}{\partial t} \qquad \boldsymbol{x} \in \Omega \subset \mathbb{R}^3 \tag{1.24}$$

$$n \times \boldsymbol{E} = \boldsymbol{0} \qquad \text{at } \partial\Omega \times (0, \mathrm{T}) \tag{1.25}$$

$$\boldsymbol{E}|_{t=0} = \boldsymbol{E}^0 \qquad \text{in } \Omega \tag{1.26}$$

This is only one of many formulations that can be used in working with magnetoquasistatic problem. We can also solve the problem in magnetic intensity $\boldsymbol{H}$ or use one of many vector or scalar potentials (Šolín et al., 2003).

1.6 Singularity removal

In the previous formulation we modeled the electric field directly by using impressed current source inside the domain. The straightforward formulation and implementation are the main advantages of this so-called *total field* approach.

Linearity of Maxwell's equations allows us to split the total field into two parts,

$$\boldsymbol{E} = \boldsymbol{E_0} + \boldsymbol{E_1}, \quad \boldsymbol{H} = \boldsymbol{H_0} + \boldsymbol{H_1}. \tag{1.27}$$

The *primary* electric field $\boldsymbol{E_0}$ and the *secondary* electric field $\boldsymbol{E_1}$.

The primary fields used in geophysics are usually magnetic or electric dipoles or plane waves which can be computed analytically. It is not necessary to model the singular source directly and, therefore, this procedure is also sometimes called singularity removal (Zhdanov, 2009).

Primary field in our work is the field driven by the dipole source embedded in the infinite isotropic homogeneous conductive matter with conductivity σ_0. On the other hand the secondary field is driven only by the conductivity inhomogeneities.

We start by writing down Faraday's and Ampere's laws in the terms of total fields as

$$\nabla \times \boldsymbol{E} = -\mu\frac{\partial \boldsymbol{H}}{\partial t}, \tag{1.28}$$

$$\nabla \times \boldsymbol{H} = \boldsymbol{j^g} + \sigma\boldsymbol{E}. \tag{1.29}$$

We can assume that the primary fields $\boldsymbol{E_0}$, $\boldsymbol{H_0}$ are either known analytically or we are able to compute them by some different numerical method, e.g. integral equation. The primary fields are also a solution to Maxwell's equations and have to obey Faraday's and Ampere's laws. We have

$$\nabla \times \boldsymbol{E_0} = -\mu \frac{\partial \boldsymbol{H_0}}{\partial t}, \tag{1.30}$$

$$\nabla \times \boldsymbol{H_0} = \boldsymbol{j^g} + \sigma_0 \boldsymbol{E_0}. \tag{1.31}$$

Subtracting (1.30) from (1.28) and (1.31) from (1.29) we have

$$\nabla \times \boldsymbol{E_1} = -\mu \frac{\partial \boldsymbol{H_1}}{\partial t}, \tag{1.32}$$

$$\nabla \times \boldsymbol{H_1} = \sigma \boldsymbol{E} - \sigma_0 \boldsymbol{E_0}. \tag{1.33}$$

By introducing *anomalous conductivity*

$$\sigma_1 = \sigma - \sigma_0 \tag{1.34}$$

we have

$$\nabla \times \boldsymbol{E_1} = -\mu \frac{\partial \boldsymbol{H_1}}{\partial t}, \tag{1.35}$$

$$\nabla \times \boldsymbol{H_1} = \sigma \boldsymbol{E_1} + \sigma_1 \boldsymbol{E_0}. \tag{1.36}$$

We supposed that we know or we can cheaply compute the vector $\boldsymbol{E_0}$. The $\sigma_1(\boldsymbol{x})$ can be trivially computed from (1.34) in every single point $\boldsymbol{x} \in \Omega$. It has the properties of source and we introduce an *anomalous source*

$$\boldsymbol{j^{g1}} = \sigma_1 \boldsymbol{E_0}. \tag{1.37}$$

Finally, we have

$$\nabla \times \boldsymbol{E_1} = -\mu \frac{\partial \boldsymbol{H_1}}{\partial t}, \tag{1.38}$$

$$\nabla \times \boldsymbol{H_1} = \sigma \boldsymbol{E_1} + \boldsymbol{j^{g1}}. \tag{1.39}$$

The equations (1.38 - 1.39) have the same form as the original Faraday's and Ampere's laws. Only difference is that instead of the total field $\boldsymbol{E_1}$ they describe relations between the secondary fields $\boldsymbol{E_1}$ and $\boldsymbol{H_1}$. Hence, we can directly write

(*Strong formulation, secondary field*): Find vector electric intensity $\boldsymbol{E_1}(x,t)$ in (0, T) such that it holds:

$$\sigma \frac{\partial \boldsymbol{E_1}}{\partial t} + \nabla \times (\mu^{-1} \nabla \times \boldsymbol{E_1}) = -\frac{\partial \boldsymbol{j^{g1}}}{\partial t} \qquad \boldsymbol{x} \in \Omega \subset \mathbb{R}^3 \tag{1.40}$$

$$n \times \boldsymbol{E_1} = \boldsymbol{0} \qquad \text{at } \partial\Omega \times (0, \mathrm{T}) \tag{1.41}$$

$$\boldsymbol{E_1}|_{t=0} = \boldsymbol{E_1^0} \qquad \text{in } \Omega \tag{1.42}$$

1.7 Remark about the eddy-currents equation

Let us repeat here again the equation (1.24). Without boundary and initial conditions it reads as

$$\sigma\frac{\partial \boldsymbol{E}}{\partial t} + \nabla \times (\mu^{-1}\nabla \times \boldsymbol{E}) = -\frac{\partial \boldsymbol{j^g}}{\partial t}, \quad \boldsymbol{x} \in \Omega \subset \mathbb{R}^3.$$

First, let us focus on the constant σ that stands in front of the time derivative $\frac{\partial \boldsymbol{E}}{\partial t}$. This is the conductivity of the medium introduced by Ohm's law in (1.18). In insulating medium this constant can be very low or vanish completely. Depending on this constant our equation shows different behavior in the conducting ($\sigma > 0$) and non-conducting ($\sigma = 0$) region. If the region is *non-conducting*, σ will diminish the time dependency and the parabolic equation (1.24) degenerate to a stationary elliptic equation. Furthermore, we can see[6] that in that case the equation is not even uniquely solvable. It can be shown that when other Maxwell equations are added the system retains well-possedness (Monk, 2003). We will not deal with this case in our formulation.

1.8 Solving an Initial Value Boundary Problem

The formulations (1.24-1.26) or (1.40-1.42) are an initial value boundary problem IVBP-S:

$$\sigma\frac{\partial \boldsymbol{E}}{\partial t} + \nabla \times (\mu^{-1}\nabla \times \boldsymbol{E}) = -\frac{\partial \boldsymbol{j^{g1}}}{\partial t} \qquad \boldsymbol{x} \in \Omega \subset \mathbb{R}^3 \tag{1.43}$$

$$n \times \boldsymbol{E} = \boldsymbol{0} \qquad \text{at } \partial\Omega \times (0, \mathrm{T}) \tag{1.44}$$

$$\boldsymbol{E}|_{t=0} = \boldsymbol{E}^0 \qquad \text{in } \Omega \tag{1.45}$$

In our model we suppose that there exists a lower bound for the conductivity σ_{lb} and $0 < \sigma_{lb} \leq \sigma$ holds a.e. in our simply connected domain Ω. Also, as it was discussed in the previous section, most of the materials in the ground are nonmagnetic. Therefore, $\mu = \mu_0 = \text{const.}$ in Ω, where we set the magnetic permeability to be the permeability of a vacuum.

Also we can note that because the *curl-curl* operator is not elliptic we cannot use the 'standard theory' for linear parabolic equations (Evans, 1998, Chapter 7). However, under the condition on the continuous time dependency we can, by using implicit Crank-Nicolson scheme from Chapter 2, directly discretise the strong formulation in time. This yields a boundary value problem at every time step. The resulting operator from the boundary value problem is already elliptic and the standard Lax-Milgram lemma can be used (e.g. Evans, 1998).

It is important to notice and worth repeating that the IVBP problem (1.24) cannot solve steady-steady case. In that case some other Maxwell equation has to be added to retain well-possedness. Also it can be a computational problem whenever a numerical solution is getting too close to the steady state. For discussion in geophysical literature see e.g. Smith (1996), who solves the CSEM

[6] The kernel of $\nabla \times \boldsymbol{E}$ is large. For example it contains all gradients of smooth scalar functions as $\nabla \times (\boldsymbol{E} + \nabla\phi) = \nabla \times \boldsymbol{E}$ for $\phi \in \boldsymbol{C^2}(\Omega)$, (Bossavit, 1998)

forward problem with Finite Difference in the frequency domain. In the frequency domain the same problem is observed when the frequency of the source is too low.

In the following discussion we follow a mathematical convention[7] and set $\boldsymbol{u}(\boldsymbol{x}, t) := \boldsymbol{E}(\boldsymbol{x}, t)$.

Following (Beck et al., 2000) we have a strong version of boundary value problem:

BVP-S:

$$\nabla \times \mu^{-1} \nabla \times \boldsymbol{u} + \beta \boldsymbol{u} = \boldsymbol{f} \qquad \text{in } \Omega, \tag{1.46}$$

$$\boldsymbol{u} \times \boldsymbol{n} = 0 \qquad \text{on } \partial\Omega, \tag{1.47}$$

where $\boldsymbol{u}$ is an electrical intensity at the new timestep. The right hand side $\boldsymbol{f}$ consist of the time derivative of the current density and also electrical intensity at the previous steps. The $\beta \geq \beta_0 > 0$ is a conductivity σ divided by a timestep Δt and $\mu = \mu_0^{-1} = \text{const} > 0$ is a magnetic permeability.

1.9 Weak formulation of the eddy-current equations

In the current section, we derive a weak formulation of the (1.46-1.47). We will use the weak formulation in the second part of Chapter 2 where we discuss spatial discretization. For proper formulation we will need three things: functional spaces from where we are trying to find the solution (and also some of their properties), trace theorem, and the vector Green's theorem. We start with the functional spaces.

$$H^1(\Omega) = \{u \in L^2(\Omega) : \frac{\partial u}{\partial x_i} \in L^2, 1 \leq i \leq 3\}, \tag{1.48}$$

$$\boldsymbol{H}(\text{div}; \Omega) = \{\boldsymbol{v} \in [L^2(\Omega)]^3 : \text{div } \boldsymbol{v} \in L^2(\Omega)\}, \tag{1.49}$$

$$\boldsymbol{H}(\text{curl}; \Omega) = \{\boldsymbol{v} \in [L^2(\Omega)]^3 : \text{curl } \boldsymbol{v} \in [L^2(\Omega)]^3\}. \tag{1.50}$$

It can be shown that these spaces when equipped with the matching norms

$$||v||_{H^1(\Omega)} = (||v||^2 + ||\nabla v||^2)^{\frac{1}{2}} \tag{1.51}$$

$$||\boldsymbol{v}||_{H(curl;\Omega)} = (||\boldsymbol{v}||^2 + ||\text{curl } \boldsymbol{v}||^2)^{\frac{1}{2}} \tag{1.52}$$

$$||\boldsymbol{v}||_{H(div;\Omega)} = (||\boldsymbol{v}||^2 + ||\text{div } \boldsymbol{v}||^2)^{\frac{1}{2}} \tag{1.53}$$

are Hilber spaces (Monk, 2003). The operators *grad*, *div* and *curl* are understood in a weak (distributional) sense (Bossavit, 1998, Chapter 3).

Let us define the tangential trace for the function $\boldsymbol{v}$ from $(C^1(\Omega))^3$ as:

$$\boldsymbol{\gamma_t}(\boldsymbol{v}) = (\boldsymbol{n} \times \boldsymbol{v}) \tag{1.54}$$

then the following theorem holds:

[7] We prefer this convention also because it can guide us in the question '*What are we talking about?* '. If the 'strong' solution or the conrete physical field is discussed, we see $\boldsymbol{E}$. If the weak solution, we see $\boldsymbol{u}$. They are communicating between each other only through the boundary value problem (BVP-S) introduced on this page.

Theorem 1 (Green's theorem)**.** *Let Ω be a bounded Lipschitz domain in $\mathbb{R}^n$. Then the trace map $\boldsymbol{\gamma_t}$, which is defined classically can be extended by continuity to a continuous linear map from $\boldsymbol{H}(curl;\Omega)$ to $(L^2(\partial\Omega))^3$. Furthermore, the following Green's theorem holds for any $\boldsymbol{u} \in \boldsymbol{H}(curl;\Omega)$ and $\phi \in (H^1(\Omega))^3$:*

$$(\nabla \times \boldsymbol{u}, \phi) - (\boldsymbol{u}, \nabla \times \phi) = \langle \boldsymbol{\gamma_t}(\boldsymbol{u}), \phi \rangle, \tag{1.55}$$

where $(\cdot,\cdot)$, and $<\cdot,\cdot>$ are scalar product in $(L^2(\Omega))^3$ and $(L^2(\partial\Omega))^3$, respectively.

Proof. (Monk, 2003, Chapter 3)

Now we are justified to introduce the space $\boldsymbol{H_0}(\mathrm{curl};\Omega)$ as

$$\boldsymbol{H_0}(\mathrm{curl};\Omega) = \{\boldsymbol{v} \in \boldsymbol{H}(\mathrm{curl};\Omega) : \boldsymbol{n} \times \boldsymbol{v} = 0 \text{ on } \partial\Omega\} \tag{1.56}$$

Let us repeat here the strong form:

$$\begin{aligned} \nabla \times \mu^{-1} \nabla \times \boldsymbol{u} + \beta\, \boldsymbol{u} &= \boldsymbol{f} && \text{in } \Omega, \\ \boldsymbol{u} \times \boldsymbol{n} &= 0 && \text{on } \partial\Omega, \end{aligned}$$

The weak formulation can be found by multiplying this equation by the test function $\boldsymbol{v}$, integrating over the domain Ω and performing Green's theorem. The boundary terms introduced by Green's theorem vanish because of the homogeneous boundary conditions (1.47) and we can directly write:

BVP-W: Find $\boldsymbol{u} \in \boldsymbol{H_0}(\mathrm{curl};\Omega)$ such that for all $\boldsymbol{v}$ holds:

$$\int_\Omega \mu^{-1} \nabla \times \boldsymbol{u} \cdot \nabla \times \boldsymbol{v} \,\mathrm{dx} + \beta \int_\Omega \boldsymbol{u} \cdot \boldsymbol{v} \,\mathrm{dx} = \int_\Omega \boldsymbol{f} \cdot \boldsymbol{v} \,\mathrm{dx} \tag{1.57}$$

It is not difficult to see and it is shown by Velímský (2003) that the bilinear form $a(\cdot,\cdot)$ defined by

$$a(\boldsymbol{u}, \boldsymbol{v}) = \int_\Omega \mu^{-1} \nabla \times \boldsymbol{u} \cdot \nabla \times \boldsymbol{v} \,\mathrm{dx} + \beta \int_\Omega \boldsymbol{u} \cdot \boldsymbol{v} \,\mathrm{dx} \tag{1.58}$$

is continuous and eliptic in the curl-norm (1.52). Assuming that the right hand side bilinear form $b(\boldsymbol{v})$ defined by

$$b(\boldsymbol{v}) = \int_\Omega \boldsymbol{f} \cdot \boldsymbol{v} \,\mathrm{dx} \tag{1.59}$$

is continuous we can state that the solution is ensured by the Lax-Milgram theorem (Evans (1998)).

2. Numerical methods

In this chapter we give an overview of used numerical methods. We start by discretization of the strong initial value problem (1.24) which will lead to the series of boundary value problems (BVP-S) (1.46-1.47) with different right hand sides. Afterwards, we spatially discretise this BVP using two different Galerkin methods. Before each of these method we give a short introduction.

Let us start with the discretization of the time first.

2.1 Temporal discretization

We have initial value problem from the previous chapter (1.24):

$$\begin{aligned} \sigma\frac{\partial \boldsymbol{E}}{\partial t} + \nabla \times (\mu^{-1}\nabla \times \boldsymbol{E}) = -\frac{\partial \boldsymbol{j^g}}{\partial t} \qquad & \boldsymbol{x} \in \Omega \subset \mathbb{R}^3 \\ n \times \boldsymbol{E} = \boldsymbol{0} \qquad & \text{at } \partial\Omega \times (0, \mathrm{T}) \\ \boldsymbol{E}|_{t=0} = \boldsymbol{E}_0 \qquad & \text{in } \Omega \end{aligned}$$

It is known that for parabolic problems, the explicit schemes are unstable, unless the timestep obey Courant–Friedrichs–Lewy (CFL) condition (e.g. Hairer and Wanner, 2004) , which reads as

$$\Delta t = O(\Delta h^2). \tag{2.1}$$

Where h measure the size of the smallest cell on the used mesh. This is unfortunately[1] prohibitively expensive and, therefore implicit methods need to be used. One common choice is the θ-method.

We derive here a standard $\theta-method$ for temporal discretization (e.g. Hairer and Wanner, 2004). First we discretise the time interval $[0, T]$ with $\Delta t_n = t_n - t_{n-1}$ for $n = 1, .., N$, so that $t_0 = 0$ and $t_N = T$. We approximate the time derivative $\frac{\partial \boldsymbol{E}}{\partial t}(\boldsymbol{x}, t)$ by

the forward difference

$$\sigma\frac{\boldsymbol{E^n} - \boldsymbol{E^{n-1}}}{\Delta t_n} + \nabla \times (\mu^{-1}\nabla \times \boldsymbol{E^{n-1}}) = \left(-\frac{\partial \boldsymbol{j^g}}{\partial t}\right)^{n-1}$$

and by the backward difference

$$\sigma\frac{\boldsymbol{E^n} - \boldsymbol{E^{n-1}}}{\Delta t_n} + \nabla \times (\mu^{-1}\nabla \times \boldsymbol{E^n}) = \left(-\frac{\partial \boldsymbol{j^g}}{\partial t}\right)^{n}.$$

Next, we multiply these differences by $(1 - \theta)$ and (θ), respectively. After summation we have

[1] We will later that Discontinuous Galerkin leads to the diagonal 'mass' matrix and, therefore to the explicit discrete schemes for explicit timestepping. It is a possible big advantage to the Continuous Galerkin methods, which lead to the system of linear equations in every timestep even for explicit schemes.

$$\frac{\sigma}{\Delta t_n}\boldsymbol{E}^n + \theta\nabla\times(\mu^{-1}\nabla\times\boldsymbol{E}^n) = \\ + \theta\frac{\sigma}{\Delta t_n}\boldsymbol{E}^{n-1} - (1-\theta)\nabla\times(\mu^{-1}\nabla\times\boldsymbol{E}^{n-1}) \\ + (1-\theta)\boldsymbol{h}^{n-1} + \theta\boldsymbol{h}^n,$$

where $\boldsymbol{h}^n = \left(-\frac{\partial \boldsymbol{j}^g(t)}{\partial t}\right)^n$. Setting $\theta = 0.5$ leads to the *Crank-Nicolson* scheme. It can be shown that this implicit scheme is second order in time accurate (Hairer and Wanner, 2004).

$$\frac{\sigma}{\Delta t_n}\boldsymbol{E}^n + \frac{1}{2}\nabla\times(\mu^{-1}\nabla\times\boldsymbol{E}^n) = \\ + \frac{\sigma}{\Delta t_n}\boldsymbol{E}^{n-1} - \frac{1}{2}\nabla\times(\mu^{-1}\nabla\times\boldsymbol{E}^{n-1}) \\ + \frac{1}{2}(\boldsymbol{h}^{n-1} + \boldsymbol{h}^n)$$

In the end we multiply previous equation by factor 2 and set

$$\beta = \frac{2\sigma}{\Delta t_n}. \tag{2.2}$$

Then, we switch the first two terms and we have

$$\beta\boldsymbol{E}^n + \nabla\times(\mu^{-1}\nabla\times\boldsymbol{E}^n) = \\ + \beta\boldsymbol{E}^{n-1} - \nabla\times(\mu^{-1}\nabla\times\boldsymbol{E}^{n-1}) \\ + (\boldsymbol{h}^{n-1} + \boldsymbol{h}^n). \tag{2.3}$$

Now we denote the whole right hand side (RHS) of (2.3) as

$$\boldsymbol{f}^n = \beta\boldsymbol{E}^{n-1} - \nabla\times(\mu^{-1}\nabla\times\boldsymbol{E}^{n-1}) + (\boldsymbol{h}^{n-1} + \boldsymbol{h}^n). \tag{2.4}$$

Terms on the right side of (2.4) are known from the previous steps. We can treat the forcing term $\boldsymbol{h} = -\frac{\partial \boldsymbol{j}^g}{\partial t}$ on the right hand side of (2.4) also by Crank Nicolson, keeping the same order of approximation.

Now, combining this discrete aproximation of derivative $-\frac{\partial \boldsymbol{j}^g}{\partial t}$, together with previous results (2.3) and (2.4), we can write the formula for the series of BVP-S problems as

Let $[0,T]$ be a time interval. Let $\Delta t_n = t_n - t_{n-1}$ for $n = 1,..,N$, so that $t_0 = 0$ and $t_N = T$. For $n = 1,..,N$ find $\boldsymbol{E}^n$ such that

$$\beta\boldsymbol{E}^n + \nabla\times(\mu^{-1}\nabla\times\boldsymbol{E}^n) = \boldsymbol{f}^n, \quad \text{where} \tag{2.5}$$

$$\boldsymbol{f}^n = \beta\boldsymbol{E}^{n-1} + \nabla\times(\mu^{-1}\nabla\times\boldsymbol{E}^{n-1}) + \frac{1}{\Delta t_n}(\boldsymbol{j}^{n-1} - \boldsymbol{j}^n) \tag{2.6}$$

specifically, for the initial condition we have

$$\boldsymbol{f}^1 = \beta\boldsymbol{E}^0 + \nabla\times(\mu^{-1}\nabla\times\boldsymbol{E}^0) + \frac{1}{\Delta t}(\boldsymbol{j}^0 - \boldsymbol{j}^1) \tag{2.7}$$

It is worth to notice that the initial conditions consist of initial value field $\boldsymbol{E}(\boldsymbol{x}, t = 0)$ but also the given current fields $\boldsymbol{j^g}(\boldsymbol{x}, t = 0)$ and $\boldsymbol{j^g}(\boldsymbol{x}, t = t_1)$. They are not independent but obey the condition (1.21), which reads:

$$\nabla \cdot (\boldsymbol{j^g} + \sigma \boldsymbol{E}) = 0.$$

We conclude this section with the hypothesis that this is the most probable source of problems, when the secondary formulation was used in the computation in Chapter 4. We refer to Chapter 4 for further discussion.

2.2 Spatial discretization

In the rest of this chapter we will be discussing two different discretization. First we will review conforming Nédélec Finite elements. The discontinuous version will be discussed in the next section where we also discuss different discontinuous schemes, that could be used and provide reasoning about our particular choice. It is not possible to treat here the complete theory. Therefore, we will only provide the basic overview and discuss connections and differences between both of these approaches. First we will show the difference between conforming and nonconforming method - Discontinuous Galerkin.

Now, let us repeat here our weak formulation of the continuous boundary value problem from the end of Chapter 1. For better clarity of the ideas we will slightly change notation and denote $\boldsymbol{V} = \boldsymbol{H_0}(\mathrm{curl}, \Omega)$:

BVP-W: Find $\boldsymbol{u} \in \boldsymbol{V}$ such that

$$a(\boldsymbol{u}, \boldsymbol{v}) = f(\boldsymbol{v}), \quad \forall \boldsymbol{v} \in \boldsymbol{V}$$

The functional space $\boldsymbol{V}$ is infinite dimensional. The standard idea behind the *conforming* Galerkin approximation is to keep the bilinear form $a(\boldsymbol{u}, \boldsymbol{v})$ the same and only choose some subspace $\boldsymbol{V_h} \subset \boldsymbol{V}$ solve the problem:

BVP-CG: Find $\boldsymbol{u_h} \in \boldsymbol{V_h}$ such that

$$a(\boldsymbol{u_h}, \boldsymbol{v_h}) = f(\boldsymbol{v_h}), \quad \forall \boldsymbol{v_h} \in \boldsymbol{V_h} \tag{2.8}$$

the advantage of this approach is that if some mathematical property (e.g. ellipticity of the bilinear form $a(\cdot, \cdot)$) holds on the bigger, infinite dimensional space $\boldsymbol{V}$ it has to hold also on the smaller subspace and we have automatically existence and uniqueness. On the other hand Discontinuous Galerkin methods[2] are solving the following problem:

BVP-DG: Find $\boldsymbol{u_h^{DG}} \in \boldsymbol{U_h}$ such that

$$a_h(\boldsymbol{u_h^{DG}}, \boldsymbol{v_h}) = f(\boldsymbol{v_h}), \quad \forall \boldsymbol{v_h} \in \boldsymbol{U_h},$$

we see that two things has changed comparing to the previous case. First, now the space $\boldsymbol{U_h}$ is not a subspace of the continuous problem $\boldsymbol{U_h} \not\subset \boldsymbol{V}$ for the test

[2] At least in their 'primal' form. See the discussion in section 2.4 about why we are using primal and not the more general 'flux' form.

and trial functions. And second, we are now using a bilinear form $a_h(\cdot,\cdot)$ instead of $a(\cdot,\cdot)$. In general, the bilinear form $a_h(\cdot,\cdot)$ does not have to be even elliptic. Properties of $a_h(\cdot,\cdot)$ have to be investigated separately.

This was a fairly abstract point of view. Now, for the time being we skip discussion about the spaces $\boldsymbol{V_h}$ and $\boldsymbol{U_h}$ and proceed directly to matrices.

2.2.1 Matrices

Provided that $\{\boldsymbol{\phi_i}\}$ are basis of V_h we can (e.g. Brenner and Scott, 2007) expand the 'trial' functions u_h, to this basis. We have

$$\boldsymbol{u_h} = \sum_j u_j \boldsymbol{\phi_j}. \tag{2.9}$$

Now we insert this expansion to the BVP-CG problem (2.8) from Chapter 2 we have:

BVP-W: Find $\boldsymbol{u_h} \in \boldsymbol{V_h} \subset \boldsymbol{H_0}(\mathrm{curl};\Omega)$ such that for all $\boldsymbol{v} \in \boldsymbol{V_h}$ holds:

$$\int_\Omega \mu^{-1} \nabla \times \boldsymbol{u_h} \cdot \nabla \times \boldsymbol{v}\,\mathrm{dx} + \beta \int_\Omega \boldsymbol{u_h} \cdot \boldsymbol{v}\,\mathrm{dx} = \int_\Omega \boldsymbol{f} \cdot \boldsymbol{v}\,\mathrm{dx} \tag{2.10}$$

or in the bilinear form:

$$a(\boldsymbol{u_h}, \boldsymbol{v_h}) = f(\boldsymbol{v_h})$$

$$a\left(\sum_j u_j \boldsymbol{\phi_j}, \boldsymbol{v_h}\right) = f(\boldsymbol{v_h})$$

By letting $v = \boldsymbol{\phi_i}$ we have n conditions

$$\sum_j u_j a(\boldsymbol{\phi_j}, \boldsymbol{v_h}) = f(\boldsymbol{v_h}), \quad \forall \boldsymbol{v_h} \in \boldsymbol{V_h}.$$

Now we can define new matrices and vectors

$$M_{ij} = \int_\Omega \beta \boldsymbol{\phi_i} \cdot \boldsymbol{\phi_j}\,\mathrm{dx}, \tag{2.11}$$

$$S_{ij} = \int_\Omega \mu^{-1} (\nabla \times \boldsymbol{\phi_i}) \cdot (\nabla \times \boldsymbol{\phi_j})\,\mathrm{dx}, \tag{2.12}$$

$$g_i = \int_\Omega \boldsymbol{f} \cdot \boldsymbol{\phi_i}\,\mathrm{dx}, \tag{2.13}$$

$$A_{ij} = M_{ij} + S_{ij} \tag{2.14}$$

And we see that the 2.8 reduce to the linear algebra system:

$$Au = f \tag{2.15}$$

2.3 Galerkin discretization

Now let us return to the question of spaces for $\boldsymbol{V_h}$ from the conforming Galerkin approximation stated in section 2.2. We repeat again (2.8) which reads:

BVP-CG: Find $\boldsymbol{u_h} \in \boldsymbol{V_h}$ such that

$$a(\boldsymbol{u_h}, \boldsymbol{v_h}) = f(\boldsymbol{v_h}), \quad \forall \boldsymbol{v_h} \in \boldsymbol{V_h}$$

In the previous section we showed that this leads to a system of linear equations, provided we have the bases $\boldsymbol{\phi_i}$. Now the only missing thing are some bases, that we can use. The systematic way how to create such bases is by using a finite element method (FEM) (e.g. Brenner and Scott, 2007).

As we discussed in the setion 2.2, the key property of the basis is the conforming property which ensures that $\boldsymbol{V_h} \subset \boldsymbol{V}$ as discussed in the beginning of section 2.2. One such basis provides Nédélec elements.

2.3.1 Conforming Galerkin method

Brief overview of Nédélec elements

In 1980, Nedelec (1980) introduced first[3] family of finite elements in $\mathbb{R}^n$, one of which, called *edge elements*, conforms to the function space $\boldsymbol{H}(curl)$. This family of finite elements has a very important property. The tangential component of a approximated vector function is continuous across the element. boundaries[4]. On the other side the normal component of a approximated vector can vary across the element boundary. This property is necessary for exact modeling jumps of electric field $\boldsymbol{E}$ and magnetic field $\boldsymbol{H}$. We will only discuss here a small subset of the necessary theory. Treatment of these elements can be found in the books Monk (2003), Šolín et al. (2003) and Bossavit (1998).

First, we introduce the mathematical definition of the finite element from Šolín et al. (2003).

Definition 1 (Finite element)**.** *Finite element is the triad (K, P, Σ), where*

- *K is a domain in $\mathbb{R}^3$ - we will discuss only the case of K being tetrahedron or cuboid.*
- *P is a space of polynomials on K of dimension dim(P) = N_P*
- *$\Sigma = \{L_1, L_2, \ldots, L_{N_P}\}$ is a set of linear forms*

$$L_i : P \to \mathbb{R}, \;\; i = 1, 2, \ldots, N_P.$$

The elements of Σ are called degrees of freedom (DOF).

The domain K, space P and linear forms Σ from Finite Element cannot be chosen arbitrarily but need to be compatible to each other and also with the local functional space $V_h(K)$. The compatibility condition between the set of DOFs Σ

[3]"first" is used to distinguish these finite elements from the later paper by Nédélec (1986)

[4]Nedelec (1980) shows that this is also *sufficient* condition for conformity to $H(curl, \Omega)$

and the polynomial space P is called *unisolvency* (Šolín et al., 2003). We suppose that our element is unisolvent.

In the lowest order Nédélec elements Nedelec (1980), discussed lengthly in (Bossavit, 1998, Chapter 5), their space P consists of the polynomial functions that have constant tangential component on the edges of element. Their explicit formula for cuboid element can be found in (Jin, 2002). Also it can be shown that these bases are divergence-free. Therefore, the global function $\boldsymbol{u_h}$ that is approximated by these functions has to be locally divergence-free (Jin, 2002). This is a key property for treating the problem of 'spurious solutions' (Jin, 2002).

2.4 Discontinuous Galerkin method

In this chapter we first introduce Discontinuos Gelerkin method and then review its possible use to Maxwell's equations.

Overview

Discontinuous Galerkin finite element method (DG-FEM or only *DG*) combines the ideas and techniques from Finite Element and *Finite Volume* (FVM) methods (Hesthaven and Warburton, 2007). DG was first used to solve first-order hyperbolic neutron transport equation in the seventies (Reed and Hill, 1973). Being based on discontinuous finite element spaces, DG methods have many advantageous properties. It can easily handle meshes with hanging nodes (see Figure 2.1), meshes can consists of the elements of different shapes and local spaces can be easily of different order on various elements leading to p-adaptivity(Schneebeli, 2006). This mesh and order flexibility designates DG as an ideal candidate for *hp-adaptivity* [5].

There are two approaches that are commonly used in the discretization of a second order elliptic operator. One comes from interior penalty methods and is usually called *primal* discretization. The second option is to rewrite the high spatial derivative as a system of first-order equations which leads to the term *numerical fluxes* (Hesthaven and Warburton, 2007). To distinguish it from the first approach we will call it a *numerical-flux formulation*. It was showed on the example of Poisson equation in Arnold et al. (2002) that all the primal discretization can be developed from a flux formulation by choosing different numerical fluxes.

Nowadays it is a popular choice for computing linear and nonlinear conservation laws in e.g. elasticity, shallow water equations or gas dynamics and can be viewed as an high order generalization of finite volume methods (Feistauer et al. 2003; Hesthaven and Warburton 2007). An comprehensive review in the development of the DG can be found in the first chapter of Hesthaven and Warburton (2007).

[5] This is many times repeated in the introduction to the most of the articles about DG. Unfortunately for the modeling of curl-curl operator in Maxwell equations this is a rather simplifying point as we note later.

2.4.1 Discontinuos Galerkin for the Maxwell Equations

The reviewing possible choices took considerable amount of time. Therefore, we would like to provide here a reasoning behind the choice of our particular DG method. The author of this work tried the best but he is not an expert and the following review could be biased by the availability of sources he had access to. They are cited in the next paragraphs.

The Maxwell equations in magnetoquasistatic approximation have parabolic (or elliptic) character. After reviewing the literature (e.g. especially Hesthaven and Warburton (2007), Pietro and Ern (2011), Feistauer et al. 2003) and articles (Grote et al. (2007)), Grote et al. (2008))) we concluded that for these equations there is no apparent advantage. The places where it could be competitive for Maxwell's equations are *hp-FEM* methods (Pesch et al., 2007) and explicit-time domain simulations (Hesthaven and Warburton, 2007).

The *hp-FEM* methods are methods that combine so called (h-adaptation), which that is adapting mesh and (p-adaptation), which is locally varying the order of polynomials that approximate the solution on the element. This is a hard task (not-only) for Maxwell equations in continuous elements as the solution has to be continuous between adjacent elements. However, Šolín et al. (2003) shows that this is possible. Nevertheless, it was felt that the hp-fem in DG is too challenging goal to pursue with a very unsure end.

The second place, where the DG is a good choice are explicit-time domain simulations (Hesthaven and Warburton, 2007). By solving conservative Maxwell equations[6] (Hesthaven and Warburton, 2007) shows that high order time schemes are promising. This route was pursuaded some time. However later it became evident that it also might be fruitless in the end. The reasoning for this comes from the comparing two papers by Commer and Newman (2004) and by Um et al. (2010). Um et al. (2010) compares his FEM implicit solver running on single processor with a very effective highly parallelize scheme by Yee discussed in Chapter 1. The DG methods proposed by (Hesthaven and Warburton, 2007) are similar to Yee scheme solved by Commer and Newman (2004). Having in mind higher complexity of (any FEM) implementation we concluded that this is not very promising way for CSEM solver.

After all we decided to implement the most standard scheme for solving Maxwell's equation. This happens to be SIPG or interior penalty method. However even this approach is not without problems, when not using tetrahedral elements. This was not realized at the beginning and the library *deal.ii* was chosen as we discuss in Chapter 3.

2.4.2 Introduction

In our work we use the *Symmetric Interior Penalty Galerkin* (SIPG) method. Its application to the Maxwell equations is described in the series of articles that create a substantial part of the doctoral thesis by Schneebeli (2006). Derivation of SIPG for Maxwell equation is analogous to the one for a simple Poisson problem that is discussed extensively in many books, e.g. in Pietro and Ern (2011) or Hesthaven and Warburton (2007). The only difference are that the penalty terms

[6]Full ME without the conductivity

contain tangential jumps.

Without the derivation we state the final form of the approximating bilinear form $a^{DG}(\cdot,\cdot)$ from (Schneebeli, 2006):

$$\begin{aligned} a^{DG}_{curl}(\boldsymbol{u_h^{DG}}, \boldsymbol{v_h^{DG}}) = \quad & + \sum_K \int_K \mu^{-1}(\nabla \times \boldsymbol{v_h^{DG}}) \cdot (\nabla \times \boldsymbol{u_h^{DG}}) \,\mathrm{dx} \\ & - \sum_K \int_f [\boldsymbol{u_h^{DG}}]_T \cdot \{\{\mu^{-1}\nabla \times \boldsymbol{v_h^{DG}}\}\} \,\mathrm{ds} \\ & - \sum_K \int_f [\boldsymbol{v_h^{DG}}]_T \cdot \{\{\mu^{-1}\nabla \times \boldsymbol{u_h^{DG}}\}\} \,\mathrm{ds} \\ & + \sum_K \int_f a[\boldsymbol{u_h^{DG}}]_T \cdot [\boldsymbol{v_h^{DG}}]_T \,\mathrm{ds}, \end{aligned}$$

where $[\boldsymbol{u}]_T = \boldsymbol{n}^+ \times \boldsymbol{u}^+ + \boldsymbol{n}^- \times \boldsymbol{u}^-$ is a tangential jump and $\{\{\boldsymbol{u}\}\} = \frac{1}{2}(\boldsymbol{u}^+ + \boldsymbol{u}^-)$ is an average across the boundary element.

It corresponds only to the 'curl-curl' part of our former bilinear form from section 2.3. After adding the '$\beta\boldsymbol{u}$' part to bilinear form we can expand it similarly as we did in the section 2.3 for bilinear form $a(\cdot,\cdot)$ under the assumption that we specify the space $\boldsymbol{U_h}$. It leads to a rather large amount of terms, some of them being integrals on the faces between the elements. We will not derive them here, but rather we will discuss some practical aspects of when programming them to the deal.ii library.

2.4.3 Penalty

There is an important question of choosing the penalty parameter a from the last line of the bilinear form a_h^{DG}. When set too low the continuity of tangential on between the elements is not enforced and the quality of the solution is not satisfactory. When set too high, a condition number of the matrix A^{DG} is higher. In theory, there exists bounds on the penalty term (Schneebeli, 2006). However, for practical computation it has to be used by trial-and-error process.

2.4.4 Boundary condition

Boundary conditions are enforced only weakly in the DG. From the practical point of view, it is hard to tell if this is an advantage or not. On one side the matrix A^{DG} is not destroyed on every timestep by applying boundary conditions as in the continuous case. On the other hand this is probably outweighed by the amount of DOFs, which corresponds to boundary terms and that need to be added to the (already bigger) matrix A^{DG}. For a further discussion we refer to Pietro and Ern (2011).

2.4.5 Space of the testing functions and hanging nodes

The last two remarks of practical importance of discretization curl-curl operator need to be resolved. The first one can be stated as 'Which kind of local spaces can be used on the element?' and the second as 'Can we use hanging nodes?'.

It turns out that for hexahedral elements and SIPG formulation only the local version of Nédelec elements discussed in the previous section, provide a spurious-free approximation, the explanation (Buffa and Perugia, 2006) is out of scope of this work. Local Lagrange elements cannot be used. The question of hanging nodes is to my best knowledge discussed only for tetrahedral elements in Buffa et al. (2007) and not for hexahedral elements. However my own experience from running numerical simulations showed that hanging nodes *could not* be used on hexahedra with SIPG formulation as spurious modes appeared in the solution.

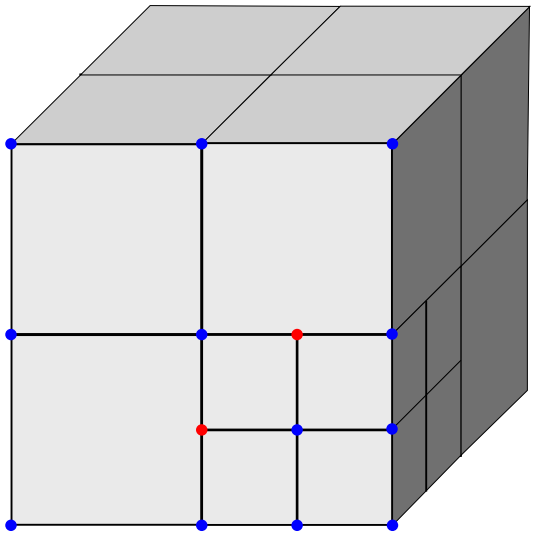

Figure 2.1: The mesh on the picture is composed from 15 cubes of two different sizes, 7 cubes with the edge $a = 2h$ and 8 cubes with the edge $a = h$. Only the nodes on the front face are emphasized by colored points. Hanging nodes are denoted by the red color, non-hanging nodes by the blue color.

It is not without theoretical interest to state that in tetrahedral elements one can indeed use hanging nodes for tetraheral elements (Buffa et al., 2007) and also local bases from Lagrange or also Nédélec elements. The later results are discussed in Buffa and Perugia 2006 and also extensively in (Hesthaven and Warburton, 2007, Chapter 9).

In the and of this chapter we will provide a brief overview.

2.5 Overview

Let us repeat our whole numerical scheme

- At the every time step we create a BVP (2.5 2.6)
- This is a strong 'BVP-S' problem stated in (1.46 - 1.47) for which we developed a weak 'BVP-W' formulation (1.57) at the end of Capter 1.
- We solve this weak Boundary Value Problem by means of conforming or nonconforming methods overviewed in this chapter.
- We proceed to the next time level and if the $t < T$ we return to the first step. Otherwise we end the algorithm.

3. Program

In this chapter we discuss an implementation of numerical methods described in the previous chapter. First, we give the reasoning behind the particular choice of the software that we used. Afterwards we give a brief summary of experiences gathered during the implementation itself.

3.1 Object-oriented library deal.ii

Programming a three dimensional time dependent finite element program can be a technically challenging task Bangerth et al. (2007). For simpler options, which would be in our case for example an implementation of the lowest order Nédélec edge element with discretization based on tetrahedral elements, it is certainly possible to develop and test a working code in the time scale of this thesis. This is probably a superior approach for the lowest order element as it allows the most flexibility and the algorithms are well documented in some more practically oriented computational electromagnetic books, e.g. Jin (2002).

For creating more advanced codes using locally adaptive (h- end especially hp-) refinement, parallelization, author of this work believe that it is better to use an underlying library in the expectation that this decision would lead, in the longer run, to a more competitive code.

There are many freely available FEM libraries, however only a handful of them are structured and documented well enough to be used outside of a team of their developers (Bangerth et al., 2007). We can vaguely distinguish two different types of FEM libraries. The ones that are employing some kind of high level language (e.g. Fenics[1]) are preferred for their "user-friendliness" as programs written in them are usually shorter and very close to the mathematical description of the problem. For developing larger and more complex programs it is often better to stay in one of the more traditional computer languages, (e.g. FORTRAN, C or C++) used in scientific computing and use a library to support such a program. Our further requirements were the support for Nédélec edge elements and discontinuous elements. For creating our program we choose to use the object-oriented library deal.ii, written in C++ and developed by Bangerth et al. (2007).

From the implementation perspective, our finite element code consists of:

- Preprocessing (creating the geometry and mesh)
- Constructing the algebraic system
- Solving the algebraic system
- Timestep
- Postprocessing

We will shortly describe these processes, without the intention of getting too deep 'into the code'.

[1] `http://fenicsproject.org/`, last visit 22. November 2012 and also Logg et al. (2012)

3.2 Preprocessing

The main part of the preprocessing is to create a good quality mesh. Our code was initially developed only on the simple geometry with homogeneous materials when the regular meshes were created within the deal.ii library. For more complicated cases of with variable conductivity or singular sources it is necessary to use irregular mesh that distributes more degrees of freedoms (DOFs) to these problematic places and less DOFs to unproblematic places.

For our more realistic scenarios, it was planned to use the program gmsh[2]. Gmsh incorporates two important parts. A simple Computer-aided design (CAD) engine that can be used to create regions with defined material properties and 3D grid generator which supports tetrahedral and hexahedral elements. However, as was discovered too late that the hexahedral support is generally not very useful for FEM modeling. This is because the automatic hexahedral mesh generator in gmsh can create a hexahedral mesh only indirectly. First, it creates a tetrahedral mesh. Afterwards each of the tetraheda is divided into four hexahedral elements as described in *'Hexing the Tet'* article by Carey (2002). Unfortunately, such hexahedra are very far from the ideal cube shape and, therefore, the mesh has an unacceptably low quality (Jin 2002; Carey 2002). Furthermore this gives rise to spurious solutions for curl-curl operator Jin (2002). As looking for an alternative was not fruitful we decided to overcome this unforeseen difficulty by programming a several routines to generate acceptable quality of mesh in deal.ii itself. The results can be seen in Figure 4.3.

This is definitely not a very satisfying solution. The problem with mesh creation can be partially mitigated by using adaptive mesh refinement.[3] However, as discussed in (Hesthaven and Warburton, 2007) an adaptive mesh refinement is a delicate thing for the time domain simulations and would be certainly out of scope of this work. Therefore, this idea is not persuaded any further in this work and is a possible direction to enhance the code.

3.3 Constructing the algebraic system

The matrix A from (2.15) is constructed by marching over the elements and numerically computing local contributions from the volume, surface and edge integrals ((2.11)-(2.13)). This is a core part of any FEM computation. Again, for a 3D problem the implementation has to be fast, which can be a challenging software problem.

Deal.ii creates an environment when common things that are needed in this marching process (Jacobian of the transformation to the master element[4], points of integration, their weights, etc.) are preprogrammed and easily available. This is the main advantage of using deal.ii especially in the higher order methods. The support of parallel computations makes this process substantially quicker on

[2] `http://geuz.org/gmsh/`, last visit 22. November 2012 and also Geuzaine and Remacle (2009)

[3] This solves only the question of effectivity. How to create an initial mesh so the faces of the mesh conforms to the inhomogeneities in conductivity σ remains unanswered.

[4] All the integrals are computing on the so-called master element as is common in FEM, more e.g. (Brenner and Scott, 2007)

modern machines.

In our problem, it is necessary to assemble the matrix A only once, at the beginning. This optimization can be used as long as the time step in the time marching process is kept constant. However in praxis, we keep only the 'mass' (2.11) and 'stiffness' (2.12) matrices in the memory unchanged and matrix A is computed as their sum at every time step. The reason is that, enforcing boundary condition changes the matrix A. This is a possible place for later optimization.

3.4 Solving the algebraic system

The matrix A from the previous step needs to be inverted. A is a sparse, symmetric, positive definite matrix with commonly around 400000 DOFs. Further, A depends on Δt_n and matrices M and S. If the mesh is constant in time and the time step is constant it would be advantageous to use some direct method and to explicitly find out A^{-1}. This is computationally expensive process because during the inversion the places in the sparse matrix that has been filled with zero values can became non-zero. Naturally for these new values a new memory has to be allocated. With enough memory and it is probably an superior approach when the matrix A is unchanged during most of the time steps. Um et al. (2010) for a similar problem, directly solves matrix with $\sim$ 200000 degrees of freedom on the computer equipped with 48 GB memory.

The other possibility is to use an iterative solver. In the case of a symmetric, positive definite matrix the so-called *conjugate gradient* (CG) method is widely used. The important measure of the invertibility of the matrix is the condition number. As noted by Avdeev (2005), the condition number in the CSEM forward problems can be very large. This causes a very slow convergence of the iterative solver and, therefore, preconditioning is necessary. Avdeev (2005) cite Jacobi, SSOR and incomplete LU to be the most favorable preconditioners. All of them are preimplemented in the *deal.ii* library. After running a number of numerical experiments we obtained the best results with SSOR. SSOR method with the relaxation parameter 1.2 is used consistently in all computations discussed in Chapter 4.

3.5 Postprocessing

Postprocessing of any 3-D problem is rather time consuming because of the amount of information on the output of the simulation. Most of the complex postprocessing programs which can produce an esthetically appealing pictures of computed reality (e.g. the Figure (4.13)) are internally working with the values of the function on the nodes. Edge elements have a support on the edges of elements. Also, shape functions of the lowest degree edge elements in hexahedral elements are a trilineal functions of place without any constraints at the end of the edge. Solution that is projected to this basis has also therefore trilinear dependency. Simple plotting all the points on some line produce a wild discontinuous plot that is very hard to comprehend. Therefore, when the value difference between two adjacent middle points is too large (see the place around 300m at Figure 4.4) we need to be sure that only the values in the middle of the edge are used.

This conceptually easy task is rather hard to do in deal.ii because this library do provide a rather complicated[5] access to the degrees of freedom.

3.6 Conclusion

Almost no program is ever finished and can be further enhanced. All the steps described in this chapter could be certainly done more effectively. At the end of all the sections we provide possible directions of further development.

[5] in the sense of layers of abstraction one needs to cross

4. Results and Discussion

4.1 General settings

In order to verify the accuracy of the solution for marine CSEM simulations, it has been compared with two other solutions with a constant frequency: an analytic infinite homogeneous space with the constant conductivity and a 2-layered model. While during a field campaign the extended area of the floor is covered by many receivers, during the testing it is convenient to have some standardized locations of the receivers. The computed results of forward modeling are usually depicted as a time series of EM fields on certain points which represent receivers. Alternatively, the distance dependency of EM fields on some distinct directions in certain time is depicted. Figure 4.1 shows these two distinct directions, a so-called *inline* and *broadside* configuration, as well as our coordinate convention[1]. In most figures, the E_x component is plotted in the inline configuration presented.

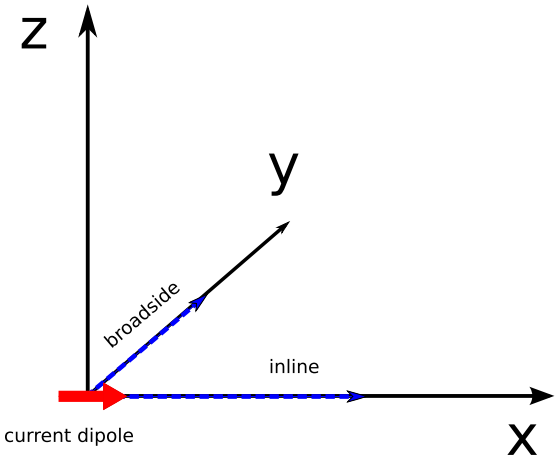

Figure 4.1: An x-oriented current dipole is placed to the center of a Cartesian coordinate system. An *inline* and *broadside* directions then coincide with the directions of growing x and y coordinates, respectively.

Unless we specifically mention otherwise we set the following for our models. We consistently used the horizontal electric current dipole (HED) with the frequency $f = 1\text{Hz}$ as the current source. The dipole was x-oriented as depicted in Figure 4.1. Every model in the following discussion is computed in the simple cuboid domain with the size of edge $a = 3100$ m.

Where applied, the following conductivity constants are used:

- Salt water: $\sigma_w = 3.3$ S.m^{-1}
- Sea floor: $\sigma_{sf} = 0.8$ S.m^{-1}
- Oil: $\sigma_{oil} = 0.001$ S.m^{-1}

[1] Our z-coordinate has exactly the opposite direction when compared to the most geophysical literature and also to the equation (1.1)

We used two different formulations discussed in Chapter 1: the primary formulation given by (1.24 - 1.26) and the secondary formulation given by (1.40-1.42). We also applied two different numerical methods discussed in Chapter 2: the Nédélec conforming Galerkin (CG) and SIPG version of Discontinuous Galerkin (DG).

In the primary formulation the source is modeled as a cube with the size of the edge 6.25m and spread across at least 4 elements in the coarsest mesh. In the secondary formulation the imaginary source is every inhomogeneity from the 'background' conductivity. The singular source is not present.

4.2 Cases

4.2.1 Homogeneous space

Figure 4.2: xz-plane cut of the homogeneous space model

First model was the simplest possible model of homogeneous space. Specially only in this model, for convenience, we use the source located in the middle of the cube. We compute only the primary formulation as the secondary formulation is trivially zero in homogeneous medium. The computed data were compared to the analytic solution (A.1) and are depicted in Figure (4.4). Additional snapshots of the primary field at different times are depicted in Figure (4.5). Note, how transient effect that is clearly visible in first two snapshots disappears for $t > 0.25$s.

We note a very good match showed in Figure 4.4 and also in Figure 4.5. But, although, the results looks good the process is costly both on the computational side and also when considering the invested human labor to create a 'proper' mesh for the computation. The main problem here is the singularity of the source field. The mesh around this singularity needs to be very dense. The use of hanging nodes is necessary to capture this adaptivity. Then, as we go further from the source the mesh should become sparser, to keep the total number of DOFs computationally feasible. Figure 4.3 shows two levels of refinement on the used

mesh. The left mesh was obtained through our simple routines in *deal.ii*. The mesh on the right of the Figure 4.3 is one time refined and is used in computations. The refined mesh contains $\sim$ 300000 DOFs. If we saw bad behavior of the solution we could not simply refine more, due to memory and computation constraints. But the new mesh had to be created. Also, only the conforming version of our finite element program could be used. The reason is the inability of our SIPG formulation of DG-method to use hanging nodes as discussed in the Chapters 2 and 3. Beside the large number of elements that were needed to be used the resulting matrix is badly conditioned resulting to a slow convergence of our iterative solver.

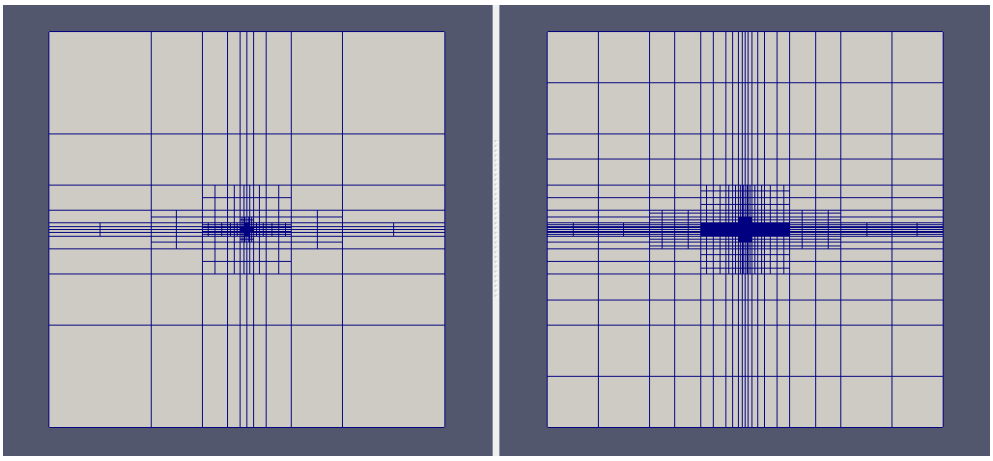

Figure 4.3: The yz-cut through the mesh used in the case of a homogeneous space. The coarse grid is on the left. Its one time globally refined grid is on the right.

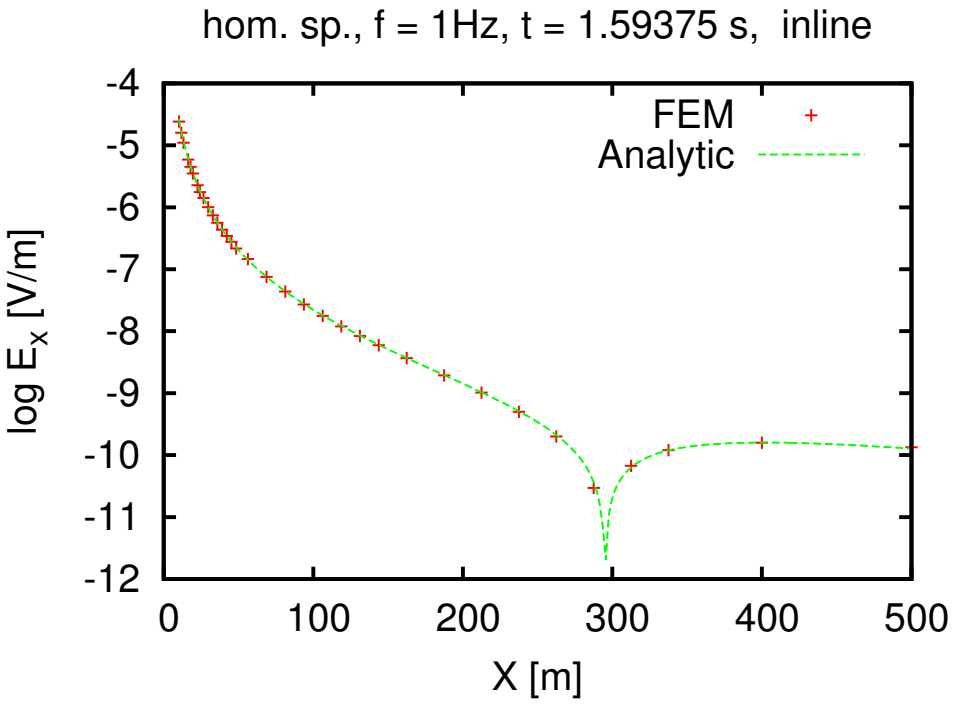

Figure 4.4: Homogenous space for a refined mesh at the $t = 1.59375$s

Figure 4.5: Time series for the homogenous space

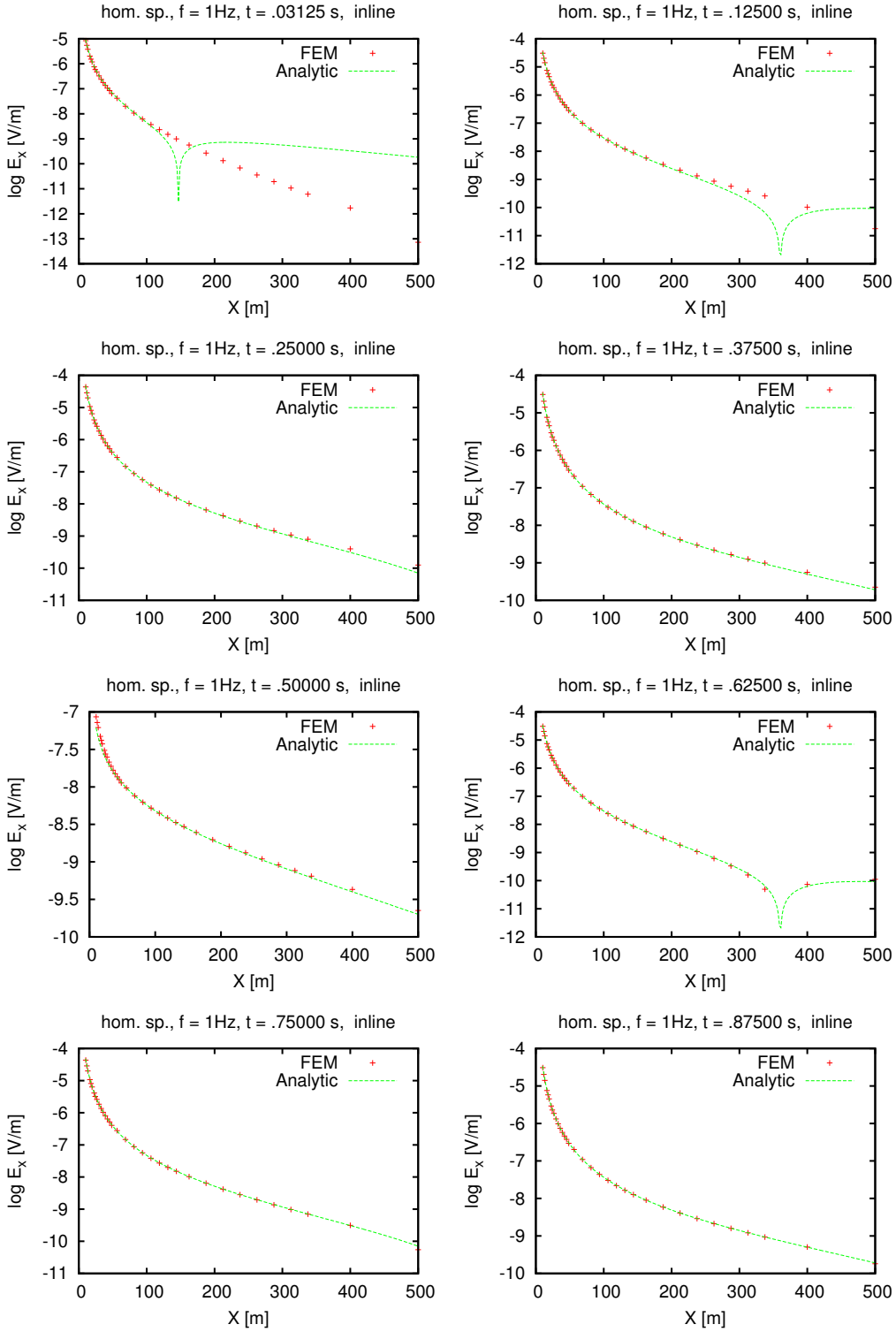

4.2.2 Sea-floor model

Figure 4.6: xz-plane cut of the sea-floor model

The first interesting model, we will investigate, is the model of the sea floor. Our domain is divided by horizontal plane going through the midpoint of the domain, dividing the domain to two horizontal layers. The top and bottom layers represent salt water and seafloor, respectively. The model is depicted on the Figure 4.6. We provide the computed results in both, primary and secondary representation. We compared our code in primary field formulation against the semianalytic forward code *Dipole1D* by Key (2009)[2]. The resulting time series is depicted in Figure 4.7. Figure 4.8 and Figure 4.9 show results computed in secondary formulation.

First we investigate the primary formulation as depicted on the timeseries in Figure 4.7. We see that the our numerical finite element solution is in a good match, after some initial phase, to the semianalytic solution by Key (2009). Also, we can clearly distinguish the response from the field produced by an homogenous space described in previous paragraph. We can therefore clearly conclude that the primary formulation is validated in the case of nontrivial double-layer space. Again, only the conforming Nédélec elements could be used.

We also computed the secondary field formulation on the seafloor model. In this case the singularity does not have to be numerically approximated and the solution exhibit good convergence as we create denser meshes. It can be seen in Figure 4.8. Meshes used for CG and DG were the same and therefore we could finally compare these two methods. We see that our continuous and discontinuous code produce comparable results on different mesh levels which suggests convergence. However, when these results are compared to the semianalytic solution by Key (2009), as can be seen in Figure 4.9, the secondary formulation (or our program) has a systematic error. This systematic error is discussed in the next section.

[2] `http://marineemlab.ucsd.edu/Projects/Occam/1DCSEM/`, last visit November 25, 2012

Figure 4.7: Time series for the seafloor model, primary formulation

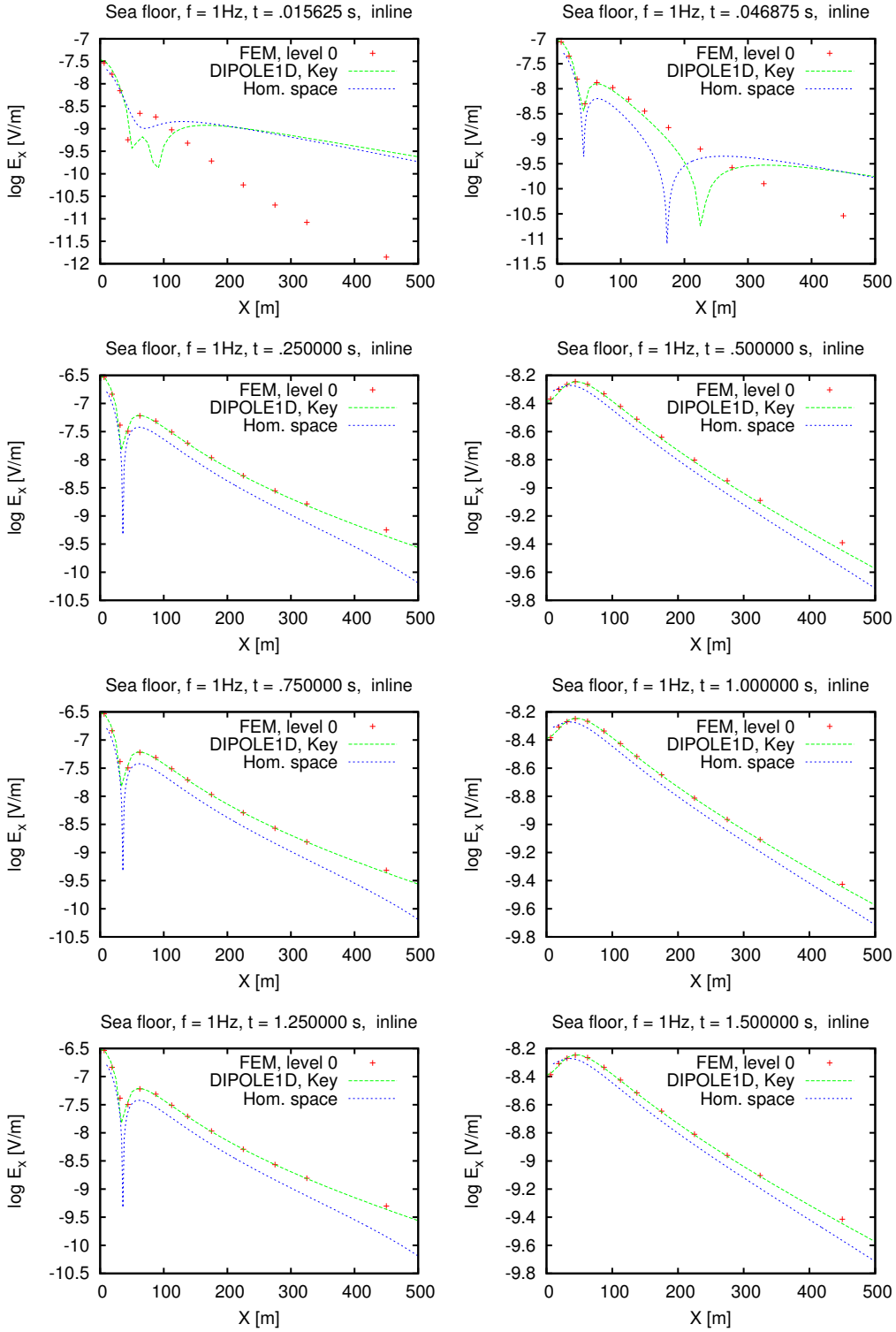

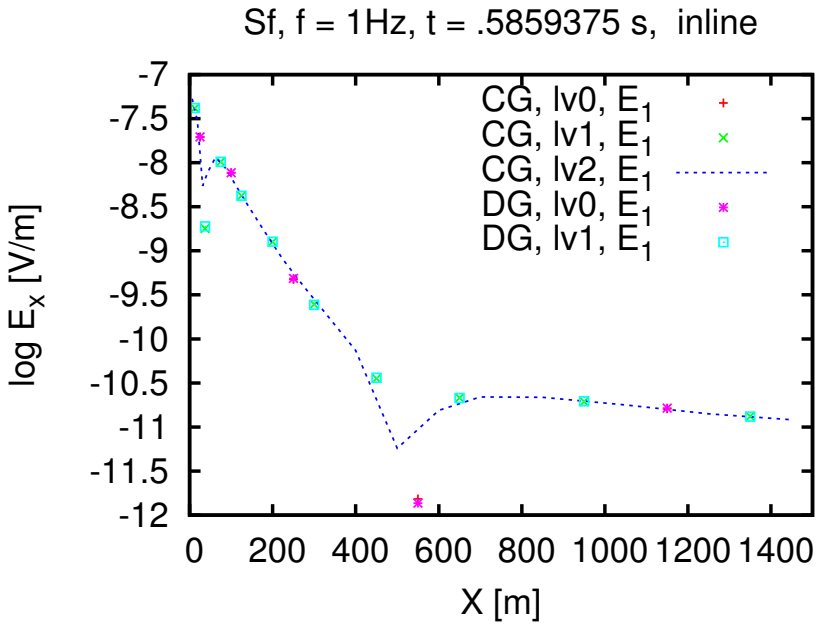

Figure 4.8: See floor model in secondary field. Series of computations on different levels of mesh and different elements. Inline electric field dependency at the time snapshot $t = 0.59$s. The blue line represents the CG solution on the finest mesh.

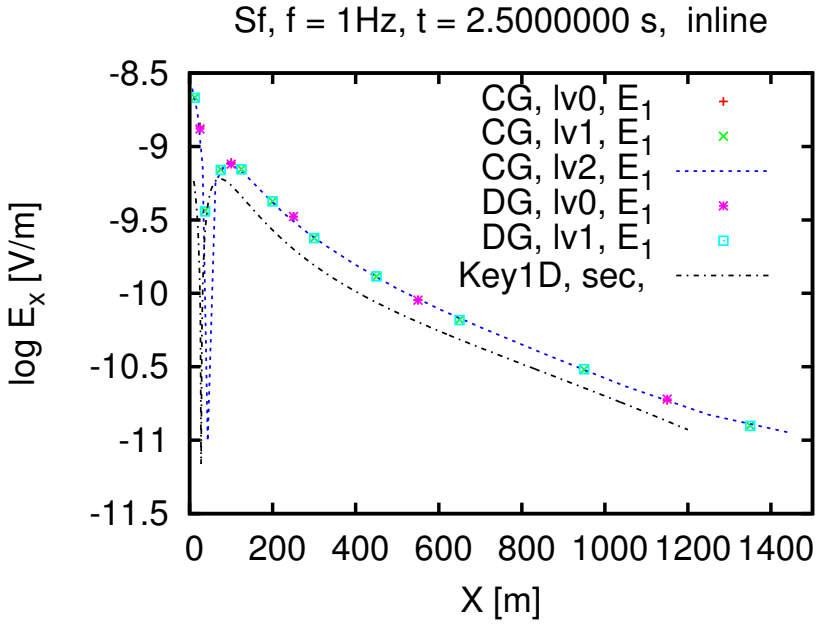

Figure 4.9: See floor model in secondary field. Series of computations on different levels of mesh and different elements. Inline electric field dependency at the time snapshot $t = 1.17$s. The blue line represents the CG solution on the finest mesh.

4.2.3 Sea-floor-oil model

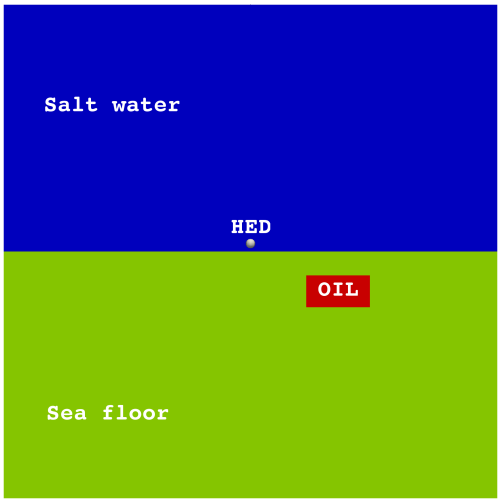

Figure 4.10: xz-plane cut of the sea-floor-oil model

The last model consists of the previous model of the sea floor with an added 3D inhomogeneity with a cuboid shape of xyz-size of 500x100x400 meters. Its location is 300 meters under the sea floor with the horizontal distance of 400 meters from the source. The inhomogeneity represents a hydrocarbon reservoir with oil of conductivity σ_O. The model is depicted on the Figure 4.10. We depict two snapshots giving on different response on the receivers on the Figure 4.11 and 4.12. We note that the measurable disturbances are observed. The last Figure 4.13 shows the distortion of the electric field owing to the inhomogeneity

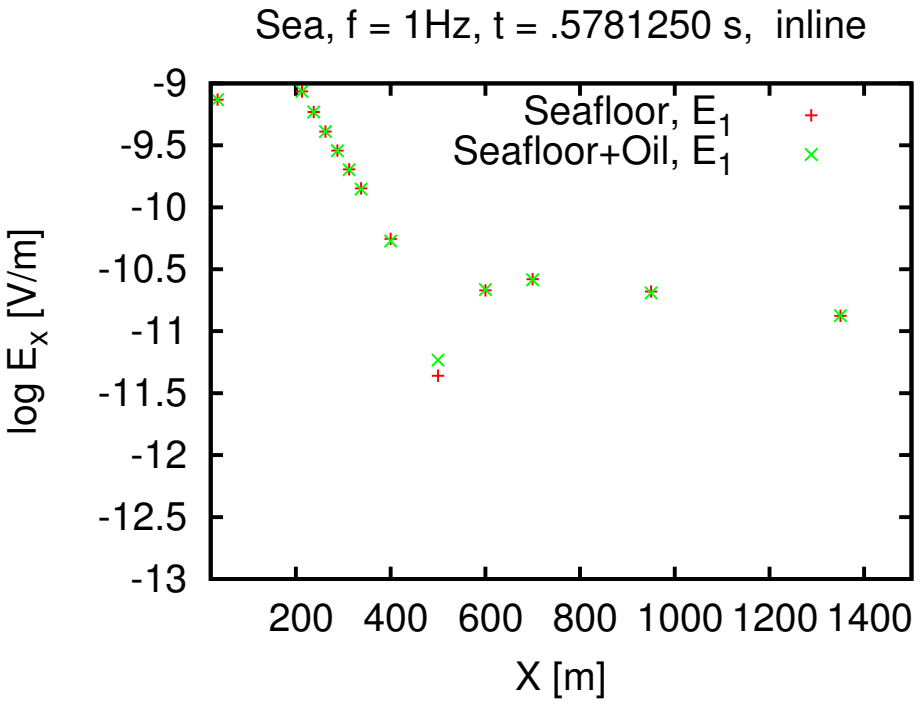

Figure 4.11: A distortion of the secondary electric field as a result of the added, highly resistive inhomogeneity.

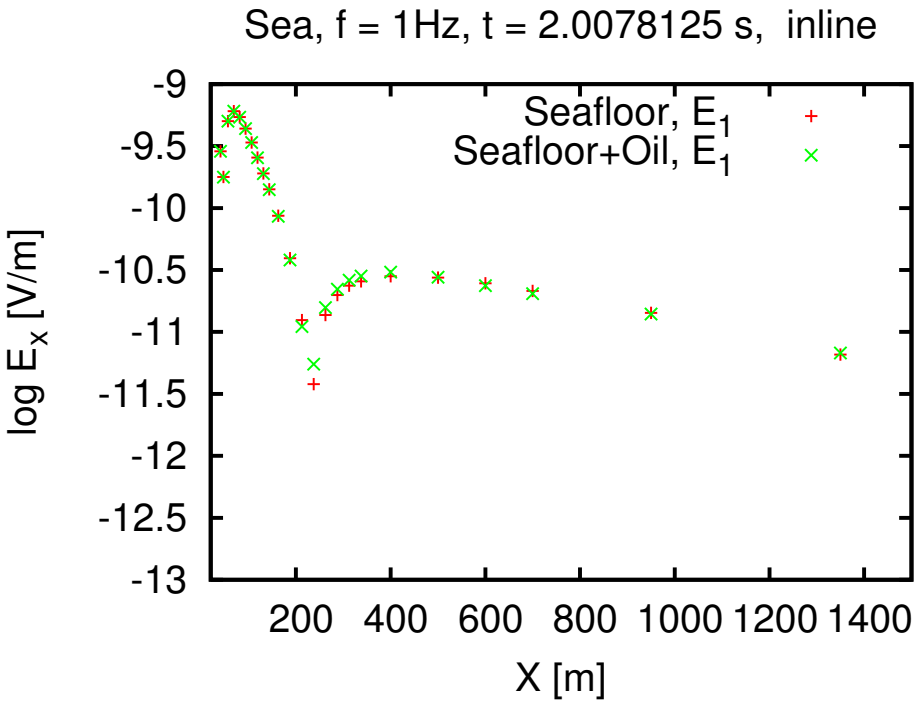

Figure 4.12: A distortion of the secondary electric field as a result of the added, highly resistive inhomogeneity.

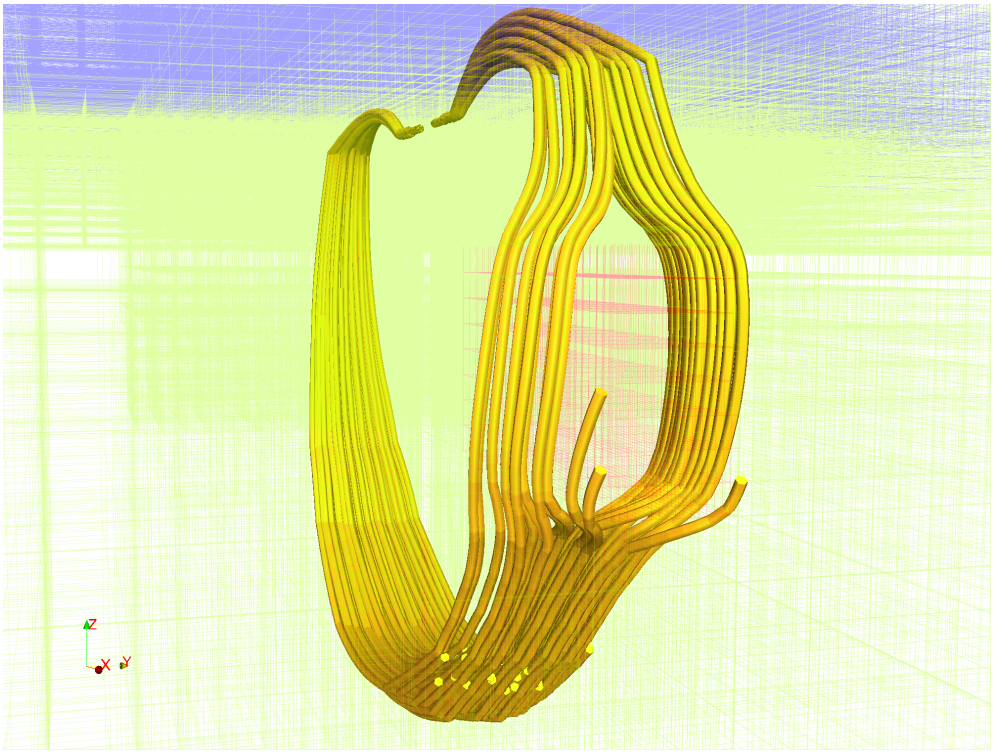

Figure 4.13: A distortion of streamlines of the secondary electric field as a result of the added, highly resistive inhomogeneity (the red part of the grid).

4.3 Discussion and conclusions

Systematic error

This systematic error observer in our solutions produced by secondary formulation with respect to the semianalytic solution by Key (2009) was investigated but the true source was not found. The problem could be caused somewhere inside our complex programs[3], that needs to be rewritten. Facing time constraint we decided to use this formulation, being the way how to compare the implemented CG and DG method. However, the probable source of error is the current conservation constraint (1.21). Closer inspection and numerical experiments suggest that the source of this systematic error might be noncompatible enforcing current and initial condition on $\boldsymbol{E}$ in divergence constraints. In the case of primal formulation this is not a problem.

Further development

The error in secondary formulation is irrelevant in cases where there is no enforcing current $\boldsymbol{j^g}$. A so called swich-off problem described in (Um et al., 2010) belongs to this category and is the possible future most exciting application of

[3]Currently totally more then 5000 lines of code become hard to maintain during an different numeric experiments that has to be done to support or disprove some hypothesis. We had to create two programs because of the different formulation, the CG and DG methods are implemented considerably different in *deal.ii*.

our code. Implementation is conceptually easy, however not straightforwardly possible (W. Bangerth, pers. comm.)[4].

We conclude that our code was validated, however in this condition it is not yet fully suitable for the practical computations where the main problem remains the mesh generation as already extensively discussed.

[4]"Implementing this, however, is a bit of of a hassle [in *deal.ii*] because [one] would need to know the numbering of degrees of freedom for both kinds of elements, etc.", W. Bangerth, the main developer of *deal.ii*

Conclusion

During the initial research about Discontinuous Galerkin methods it became clear, that the family of these methods can be inefficient in modeling Maxwell§s equation in quasistationary approximation. This problem of inefficiency was further amplified by the need of solving of a large 3D problem.

By using a finite element method library *deal.ii* we implemented a Symmetric Interior Penalty method theoretically analyzed by Schneebeli (2006). We tried to use this method for our test problem in CSEM, which involve a singular source. We observed that our solution was spoiled by the so called "spurious solutions" when using 'hanging nodes'. This was the key aspect which prevented us for using primary formulation. To treat this problem we tried a different way and developed a secondary formulation that removes the singularity as discussed in Chapter 1. By this we have been able to compute results that we provide in Chapter 3.

Beside to this unsatisfied result with our implemented version of Discontinuous Galerkin method we developed a program which by using conforming lowest order Nédélec elements was able to produce better results. We also used this program to compare these two Galerkin methods. However, the geometrical inflexibility of the used numerical *deal.ii* library and the lack of usable hexahedral generator constraints our code in regular Cartesian grid (with refinement using hanging elements). It basically mitigated the general advantage of FEM codes comparing to finite difference methods; geometrical flexibility. This price is hoped to be payed off as the deal.ii library allows us to relatively easily to use more advanced numerical techniques such as multigrid preconditioners, hp-refinement etc.

Bibliography

Arnold, D. N., F. Brezzi, B. Cockburn, and L. D. Marini (2002). Unified analysis of discontinuous galerkin methods for elliptic problems. *SIAM Journal on Numerical Analysis 39*(5), 1749.

Avdeev, D. (2005). Three-dimensional electromagnetic modelling and inversion from theory to application. *Surveys in Geophysics 26*, 767–799.

Badea, E., M. Everett, G. Newman, and O. Biro (2001). Finite-element analysis of controlled-source electromagnetic induction using coulomb-gauged potentials. *Geophysics 66*(3), 786–799.

Bangerth, W., R. Hartmann, and G. Kanschat (2007). deal.ii. A general-purpose object-oriented finite element library. *ACM Trans. Math. Softw. 33*(4), 24–es.

Beck, R., R. Hiptmair, R. Hoppe, and B. Wohlmuth (2000). Residual based a posteriori error estimators for eddy current computation. *ESAIM: Mathematical Modelling and Numerical Analysis 34*(01), 159–182.

Börner, R., O. Ernst, and K. Spitzer (2008). Fast 3-d simulation of transient electromagnetic fields by model reduction in the frequency domain using krylov subspace projection. *Geophysical Journal International 173*(3), 766–780.

Bossavit, A. (1998). *Computational electromagnetism: variational formulations, complementarity, edge elements*. Academic Press series in electromagnetism. Academic Press.

Brenner, S. and R. Scott (2007). *The Mathematical Theory of Finite Element Methods*. Texts in Applied Mathematics. Springer.

Buffa, A., P. Houston, and I. Perugia (2007). Discontinuous galerkin computation of the maxwell eigenvalues on simplicial meshes. *Journal of computational and applied mathematics 204*(2), 317–333.

Buffa, A. and I. Perugia (2006, September). Discontinuous galerkin approximation of the maxwell eigenproblem. *SIAM J. Numer. Anal. 44*(5), 2198–2226.

Carey, G. F. (2002). Hexing the tet. *Communications in Numerical Methods in Engineering 18*(3), 223–227.

Commer, M. and G. Newman (2004). A parallel finite-difference approach for 3d transient electromagnetic modeling with galvanic sources. *Geophysics 69*(5), 1192–1202.

Constable, S. (2010). Ten years of marine csem for hydrocarbon exploration. *Geophysics 75*(5), 75A67–75A81.

Constable, S. and L. J. Srnka (2007). An introduction to marine controlled-source electromagnetic methods for hydrocarbon exploration. *Geophysics 72*(2), WA3–WA12.

Edwards, N. (2005). Marine controlled source electromagnetics: Principles, methodologies, future commercial applications. *Surveys in Geophysics 26*, 675–700. 10.1007/s10712-005-1830-3.

Evans, L. (1998). *Partial Differential Equations*. Graduate Studies in Mathematics. American Math. Soc.

Everett, M. (2012). Theoretical developments in electromagnetic induction geophysics with selected applications in the near surface. *Surveys in geophysics 33*(1), 29–63.

Everett, M. and R. Edwards (1993). Transient marine electromagnetics: the 2.5-d forward problem. *Geophysical Journal International 113*(3), 545–561.

Feistauer, M., J. Felcman, and I. Straškraba (2003). *Mathematical and computational methods for compressible flow*. Numerical mathematics and scientific computation. Oxford University Press.

Geuzaine, C. and J. Remacle (2009). Gmsh: A 3-d finite element mesh generator with built-in pre-and post-processing facilities. *International Journal for Numerical Methods in Engineering 79*(11), 1309–1331.

Griffiths, D. (1999). *Introduction to electrodynamics*, Volume 3. Prentice Hall New Jersey.

Grote, M., A. Schneebeli, and D. Schötzau (2008). Interior penalty discontinuous Galerkin method for Maxwell's equations: optimal L2-norm error estimates. *IMA journal of numerical analysis 28*(3), 440–468.

Grote, M. J., A. Schneebeli, and D. Schötzau (2007, July). Interior penalty discontinuous galerkin method for maxwell's equations: Energy norm error estimates. *J. Comput. Appl. Math. 204*, 375–386.

Hairer, E. and G. Wanner (2004). *Solving Ordinary Differential Equations II: Stiff and Differential-Algebraic Problems*. Springer Series in Computational Mathematics. Springer.

Hesthaven, J. S. and T. Warburton (2007). *Nodal Discontinuous Galerkin Methods: Algorithms, Analysis, and Applications*. Springer.

Jin, J.-M. (2002). *The Finite Element Method in Electromagnetics, 2nd Edition*. Wiley-IEEE Press.

Key, K. (2009). 1D inversion of multicomponent, multifrequency marine csem data: Methodology and synthetic studies for resolving thin resistive layers. *Geophysics 74*(2), F9–F20.

Larsson, J. (2007). Electromagnetics from a quasistatic perspective. *American Journal of Physics 75*(3), 230–239.

Logg, A., K.-A. Mardal, G. N. Wells, et al. (2012). *Automated Solution of Differential Equations by the Finite Element Method*. Springer.

Monk, P. (2003). *Finite element methods for Maxwell's equations*. Numerical mathematics and scientific computation. Clarendon Press.

Nédélec, J. (1986). A new family of mixed finite elements in r3. *Numerische Mathematik 50*(1), 57–81.

Nedelec, J. C. (1980). Mixed finite elements in r. *Numerische Mathematik 35*, 315–341.

Pardo, D., L. Demkowicz, C. Torres-Verdin, and M. Paszynski (2007). A self-adaptive goal-oriented hp-finite element method with electromagnetic applications. part ii: Electrodynamics. *Computer methods in applied mechanics and engineering 196*(37-40), 3585–3597.

Pardo, D., L. Demkowicz, C. Torres-Verdín, and L. Tabarovsky (2006). A goal-oriented hp-adaptive finite element method with electromagnetic applications. part i: electrostatics. *International Journal for Numerical Methods in Engineering 65*(8), 1269–1309.

Pesch, L., A. Bell, H. Sollie, V. Ambati, O. Bokhove, and J. Van Der Vegt (2007). hpgem—a software framework for discontinuous galerkin finite element methods. *ACM Transactions on Mathematical Software (TOMS) 33*(4), 23.

Pietro, D. and A. Ern (2011). *Mathematical Aspects of Discontinuous Galerkin Methods*. Math Matiques Et Applications. Springer.

Reed, W. H. and T. R. Hill (1973). Triangular mesh methods for the neutron transport equation, technical report, la-ur-73-479. *Los Alamos Scientific Laboratory Technical*(LA-UR-73-479), 1–23.

Rieben, R. N. and D. A. White (2006, January). Verification of high-order mixed finite-element solution of transient magnetic diffusion problems. *IEEE Transactions on Magnetics 42*, 25–39.

Schneebeli, A. (2006). *Interior Penalty Discontinuous Galerkin Methods for Electromagnetic and Acoustic Wave Equations*. Ph. D. thesis, University of Basel.

Simpson, F. and K. Bahr (2005). *Practical Magnetotellurics*. Cambridge University Press.

Smith, J. (1996). Conservative modeling of 3-d electromagnetic fields, part ii: Biconjugate gradient solution and an accelerator. *Geophysics 61*, 1319.

Telford, W. M. (1990). *Applied geophysics*. Cambridge University Press.

Tezkan, B. (1999). A review of environmental applications of quasi-stationary electromagnetic techniques. *Surveys in Geophysics 20*(3), 279–308.

Um, E. and D. Alumbaugh (2007). On the physics of the marine controlled-source electromagnetic method. *Geophysics 72*(2), WA13–WA26.

Um, E. S., J. M. Harris, and D. L. Alumbaugh (2010). 3d time-domain simulation of electromagnetic diffusion phenomena: A finite-element electric-field approach. *Geophysics 75*(4), F115–F126.

Velímský, J. and Z. Martinec (2005). Time-domain, spherical harmonic-finite element approach to transient three-dimensional geomagnetic induction in a spherical heterogeneous earth. *Geophysical Journal International 161*(1), 81–101.

Velímský, J. (2003). *Electromagnetic induction in a heterogeneous Earth's mantle: Time-domain modelling*. Ph. D. thesis, Faculty of Mathematics and Physics, Charles University.

Wang, T. and G. Hohmann (1993). A finite-difference, time-domain solution for three-dimensional electromagnetic modeling. *Geophysics 58*(6), 797–809.

Yee, K. S. (1966). Numerical solution of initial boundary value problems involving maxwell's equations in isotropic media. *IEEE Trans. Antennas and Propagation*, 302–307.

Zhdanov, M. (2009). *Geophysical Electromagnetic Theory and Methods*. Methods in Geochemistry and Geophysics. Elsevier.

Šolín, P., K. Segeth, and I. Doležel (2003). *Higher-Order Finite Element Methods*. Studies in Advanced Mathematics. Taylor & Francis.

A. Electric current dipole in homogeneous space

Electric dipole with the orientation vector $\hat{\boldsymbol{d}} = (d_1, d_2, d_3,)$, $|\hat{\boldsymbol{d}}\,| = 1$ (with an impressed current $I = \mathrm{I}\,\cos(\omega t)$) in an infinite homogeneous space with a constant conductivity σ has a known analytic solution (Zhdanov, 2009). In the frequency domain for a source in the origin of the coordinate system, it can be expressed as

$$\boldsymbol{E}(\boldsymbol{r}) = \frac{\mathrm{e}^{ikr}}{4\pi\sigma}\left[\frac{-1+ikr+k^2r^2}{r^3}\boldsymbol{p} + \frac{(3-3ikr-k^2r^2)(\boldsymbol{p}\cdot\boldsymbol{r})}{r^5}\boldsymbol{r}\right].$$

where $\boldsymbol{r} = (x, y, z)$ is the position vector, $|r| = \sqrt{a^2+y^2+z^2}$ is the Euclid norm, $k = (1+i)\sqrt{\frac{\mu_0\omega\sigma}{2}}$, ω is the frequency of the source with dipole moment $\boldsymbol{p} = I\hat{\mathbf{d}}$. Where I is the impressed current. Previous equation holds in the frequency domain. To match our homogeneous initial conditions, we can express the electric field in the time-domain as

$$\boldsymbol{E}(\boldsymbol{r}, t) = Re\left\{\frac{\mathrm{e}^{-i(\omega t+\pi/2)+ikr}}{4\pi\sigma}\left[\frac{-1+ikr+k^2r^2}{r^3}\boldsymbol{p} + \frac{(3-3ikr-k^2r^2)(\boldsymbol{p}\cdot\boldsymbol{r})}{r^5}\boldsymbol{r}\right]\right\}. \quad \text{(A.1)}$$

in (A.1) we assume[1] that the current dipole is located in the origin. By changing the coordinate system using $r \to r - R'$, where R' is the position of the dipole in the new coordinate system, we receive the final formula.

[1] to make notation simpler